A NEW PROCEDURE FOR HISTORY MATCHING NATURALLY FRACTURED RESERVOIRS

A THESIS

SUBMITTED TO THE DEPARTMENT OF ENERGY RESOURCES ENGINEERING

AND THE COMMITTEE ON GRADUATE STUDIES

OF STANFORD UNIVERSITY

IN PARTIAL FULFILLMENT OF THE REQUIREMENTS

FOR THE DEGREE OF ENGINEER

Danny Hubert Rojas Paico

April 2008

Approved for the department.

_____

(Dr. Louis J. Durlofsky) Advisor

Approved for the University Committee on Graduate Studies.

Abstract

History matching, within the context of oil reservoir simulation, entails the adjustment of the geological description, or other model parameters, in order to achieve agreement between simulation predictions and actual production data. History matching of naturally fractured reservoirs is especially challenging, particularly when these models are represented using discrete fracture models (DFMs). DFMs, which represent each fracture individually, can achieve high degrees of geological realism. Standard pixel-based (i.e., Cartesian grid-based) history matching techniques cannot be applied to DFMs, however, as the DFMs are represented using generally unstructured grids. The goal of this work is to develop and test a prototype workflow for the history matching of naturally fractured reservoirs. This workflow includes two key components that are used in combination: a previously developed pixel-based history matching procedure and a calibration technique that establishes appropriate grid block parameters for the pixel models. The history matching procedure is gradient-based and applies kernel principal component analysis to represent geological models characterized by multipoint geostatistics. The calibration procedure is new and entails the use of an adjoint-based technique that determines pixel model parameters such that the flow responses from these models match those of the corresponding DFMs.

The two procedures are first applied individually for two-dimensional systems containing several wells. Waterflood examples, including the effects of capillary pressure, are considered. The methods are both shown to perform reasonably well, especially for field-level quantities, when used as stand-alone applications. The prototype history matching procedure is then applied to three different (two-dimensional) systems. The method is shown to be effective for achieving field-level

agreement in total injection rate and oil and water production rates. Degradation in the level of agreement is however observed in the well by well results. Although the general method does appear to have some advantageous features, additional investigation is required before it can be considered for practical problems.

Acknowledgments

I would like to express my deepest appreciation and gratitude to Prof. Louis Durlofsky for his mentoring and guidance in this work. Regardless of his busy schedule, he took a good amount of time to advise me, review the progress of this project, and give positive and invaluable feedback. And when things in the project seemed to collapse, he came with very creative ideas. Prof. Durlofsky was not only a great mentor for my research, but he was also a friendly career counselor. His advice will definitely endure during the course of my professional career.

Likewise, I would like to thank Prof. Jef Caers for his guidance and tutoring during a good part of my stay at Stanford. He initiated me into the fascinating world of fractured reservoirs. Thanks also go to Prof. Andre Journel and Prof. Atilla Aydin for discussing many issues with me and for motivating and fostering my interest in this kind of reservoir.

I would additionally like to specially thank Pallav Sarma for his help in this study. His adjoint implementation in GPRS enabled several aspects of this work. Many thanks also to Huanquan Pan for his technical assistance and for implementing important pieces of this work into GPRS. Similarly, I thank Mohammad Karimi-Fard for his availability for discussions.

I am also grateful to the Department of Energy Resources Engineering for the financial support provided for my study. In particular, I would like to thank the member companies of SCRF, SUPRI-B, and the Smart Fields Consortium for funding my work. I am also indebted to Chevron for providing me with a scholarship that covered some of the costs of my studies.

Additionally, I would like to thank to the Stanford Center for Computational Earth & Environmental Science (CEES) for allowing me to use their computing facilities for this research.

Finally, I would like to thank my mother Elena, who is in better life, watching me and helping me in times of difficulty; I also thank my father Linder for his constant support and encouragement in all my endeavors.

Dedicated to my family, for their encouragement in this endeavor

Contents

List of Figures

Chapter 1

1. Introduction

1.1 General background

Forecasting the production performance of a reservoir requires building reliable reservoir models with predictive capabilities. This is often done geostatistically, which means that many reservoir realizations are considered. In each model it is necessary to specify the fluid and rock properties which constitute the model parameters. The model is then input to a reservoir simulator, which simulates subsurface flow with the purpose of forecasting the production response of the reservoir under particular production scenarios (well constraints). The level of complexity of the model depends on the available data, the stage of the life of the reservoir, and the objectives of the reservoir study.

The geological model parameters, specifically porosity and permeability, are estimated using data from several sources such as seismic, logs, cores, and well testing. After the reservoir has been producing for a period of time, the production history can be used

to better constrain the reservoir model. This is accomplished by modifying the model parameters in such a way that the predicted performance matches the actual production history observed in the field. This data assimilation process is widely known in the oil industry as history matching. In previous years, and still now in many cases, the history matching process is conducted manually. That means that the model parameters are changed by trial and error until an acceptable match in production history is observed. This operation is heuristic and time consuming and it does not guarantee that a predictive reservoir model will be obtained. A more rigorous procedure for solving the history matching problem entails defining a specific inverse problem and solving it through the minimization of an objective function.

The objective function to minimize is defined as the misfit between the observed production data and the computed production response for a given set of model parameters. The set of parameters to adjust is often chosen to be the rock properties – porosity and permeability – of the reservoir. Therefore the size of the parameter space will be on the order of the number of cells in the numerical model. This problem is generally underdetermined because the number of parameters is typically much larger than the number of observations. In order to alleviate this problem, an additional term, also known as a regularization function, can be added to the original objective function.

Our focus in this work is on naturally fractured reservoirs (NFRs), which are reservoirs that contain fractures created by natural processes. Such fractures possess three basic physical characteristics: (1) they have two essentially parallel surfaces that

meet at the fracture front, (2) the surfaces are approximately planar, and (3) originally adjacent points across the fracture show small relative displacement compared to fracture length (Pollard and Segall 1987). One of the main challenges when working with NFRs is the proper modeling of fractures during the flow simulation step. The most accurate methodology for flow simulation through fractured formations is the use of discrete fracture models (DFMs), in which the rock matrix and fractures are represented explicitly using an unstructured grid (Karimi-Fard et al. 2004).

Although discrete fracture modeling can be used to obtain accurate predictions of fluid flow in fractured reservoirs for a particular geological characterization, it cannot be used directly with most existing pixel-based automatic history matching techniques (by pixel-based models we mean models described using rectangular or brick-shaped grid blocks; pixel-based history matching techniques are procedures applicable for such models). Pixel-based history matching techniques modify grid block properties using gradient information or direct evaluation of the objective function. Direct history matching of a DFM would require changing the locations of the fractures, which would then require the construction of a new grid before proceeding with the forward flow simulation. Such a procedure would slow the history matching process due to the re-gridding step (which can be challenging and time consuming), and could lead to discontinuities in computed gradients when the fracture locations are changed.

In recent work, Sarma et al. (2007, 2008) presented a new pixel-based history matching procedure which has the ability to preserve spatial structures in the geological model. This procedure uses kernel principal component analysis (KPCA) to

parameterize multipoint geostatistical models in conjunction with gradient-based minimization. The method has been applied to a variety of problems and has been shown to provide geologically consistent history matched models. Because it is a pixel-based history matching technique, we cannot directly apply this approach to our DFMs.

The goals of this study are to develop and test a prototype workflow that combines KPCA history matching with DFM representations for fluid flow in fractured reservoirs. This will require (1) application of KPCA history matching to pixel-based models with features that resemble fractures and (2) the establishment of a quantitative linkage (or calibration) between these pixel-based models and DFMs. If ultimately successful, such a workflow would provide an efficient gradient-based technique for history matching DFMs. This study presents several promising findings, but there remain key aspects of the overall workflow that require further study and improvement.

1.2 Literature review

History matching problems have been actively studied in petroleum engineering for many years. Initial work (Jacquard 1965; Chen et al. 1974; Chavent et al. 1975) addressed the estimation of permeability from pressure data, while later studies included multiphase flow effects (Wasserman et al. 1975). Because the number of unknowns was large compared to the data available, these solutions were

underdetermined. To address this issue, it was recognized that one must either decrease the number of unknowns, such as in zonation (Jahns 1966), or consider additional information. Gavalas et al. (1976) proposed the use of prior geological information as additional information. Recent work such as that of Caers (2003a) continues to emphasize that, due to the ill-posed nature of history matching problems, geological constraints are required as additional prior information. The early work of Gavalas et al. (1976), which applied a Bayesian approach, was used to estimate permeability and porosity from pressure data.

Many techniques have been developed subsequently for history matching purposes. Sarma et al. (2007) classified these algorithms into four general categories: stochastic algorithms, gradient-based methods, streamline-based techniques, and Kalman filter approaches. From this point, we follow the work of Sarma et al. (2007) in our discussion of these methods.

Widely applied stochastic algorithms include the gradual deformation method and its extensions (Roggero and Hu 1998; Le Gallo and Le Ravalec-Dupin 2000; Hu et al. 2001) and the probability perturbation method (Caers 2003b). The main advantages of stochastic algorithms are that they can preserve multipoint geostatistics (Caers 2003b), are relatively easy to implement, and that they sample globally (thus avoiding local minima). Their disadvantage is that they typically require numerous simulations for convergence (Wu 2001; Liu and Oliver 2004). To increase the efficiency of the stochastic approach, Yadav et al. (2005) proposed a methodology to delineate multiple reservoir domains and to then perform the history match in a distributed computing

environment. Another stochastic method that aimed to reduce computational time is the procedure of Sahni and Horne (2006), in which wavelet transforms of the parameter distribution are applied. Efficiency was achieved by decoupling the wavelet coefficients into sets of history-matching and geologic coefficients.

Gradient-based history matching techniques using adjoints (optimal control theory) were originally considered by Chen et al. (1974) and Chavent et al. (1975). These early studies were applied to single-phase flow problems. Extensions of these adjoint models for multiphase history matching were introduced subsequently (Wasserman et al. 1975; Watson et al. 1980; Lee and Seinfeld 1987; Yang and Watson 1988; Zhang and Reynolds 2002). The gradient of the objective function required in the gradient-based methods can be computed using the adjoint method or the sensitivity coefficient method among others. The sensitivity coefficient method uses the gradient of the objective function to calculate the Hessian. This Hessian matrix is used with second order optimization algorithms such as Gauss-Newton. Sensitivity coefficients have been computed for single-phase problems (Carter et al. 1974; He et al. 1997) and multiphase flow problems (Tang et al. 1989). Several works (Anterion et al. 1989; Bissell 1994a; Bissell et al. 1994b; Landa et al. 1996; Wu et al. 1999; Li et al. 2001; Wu 2001) describe the computation of sensitivity coefficients using the adjoint or gradient of the simulator. The limitations of gradient-based methods are the need to generate the gradient simulation code, the convergence to a local minimum, and limitations in terms of capturing realistic geology.

The gradient-based methods described above require working directly with the simulation code. To circumvent this complication, Gao et al. (2007) proposed a simultaneous perturbation stochastic approximation (SPSA) method to generate a down hill search direction at each iteration. Capturing realistic geology was addressed with the pilot point method revisited by Bissell et al. (1997); their method combines gradient information with geostatistical constraints.

Streamline-based history matching methods have been presented by several authors (Vasco et al. 1998; Wen et al. 1998; Wang and Kovseck 2001; Wu and Datta-Gupta 2002; Agarwal and Blunt 2003; Caers 2003b; Cheng et al. 2004). These methods are attractive because the forward simulation can be performed efficiently and because sensitivity coefficients can be computed with only one forward simulation. A main limitation of these methods is their lack of generality in terms of reservoir flow modeling. In addition, many existing formulations do not honor multipoint geostatistics.

Kalman filter based approaches are currently under active investigation and have been reported to be very efficient for real time history matching (Gao et al. 2005; Liu and Oliver 2005; Dong et al. 2006; Wen and Chen 2007). Key advantages of this method are its ease of implementation and its efficiency. The limitation is that current implementations only preserve two-point geostatistics.

Sarma et al. (2007) proposed a gradient-based technique that applies kernel principal component analysis (KPCA) to represent multipoint geostatistics. This approach

generalizes earlier techniques (Gavalas et al. 1976; Oliver 1996; Reynolds et al. 1996) that represent two-point geostatistics using Karhunen-Loeve expansions (or PCA). KPCA procedures apply PCA in a high-order feature space. Using either PCA or KPCA, the geological realization is represented in terms of a small set of parameters ξ. Gradients are then computed with respect to ξ. The models obtained are geologically consistent, and the history matching process is efficient. Our intent here is to use KPCA-based history matching as one component of our workflow.

We now briefly discuss previous work on the modeling of naturally fractured reservoirs. Many modeling procedures apply dual-porosity representations (e.g., Warren and Root 1963; Kleppe and Morse 1974; Kazemi et al. 1976) which distinguish between fracture and matrix rock regions. These methods use transfer functions to account for fluid exchange between fractures and matrix. Subsequent work by Gilman and Kazemi (1983) addressed some practical aspects of the simulation of dual-porosity systems. One such limitation is that the fracture systems are often idealized as very regular patterns, although studies (e.g., Laubach 1991) have shown that they can be very irregular and/or disconnected. A related limitation is the difficulty of accurately evaluating the transfer function for complex fracture distributions.

To address these issues, some recent efforts have aimed at representing the fractures individually. These approaches are known as discrete fracture models (DFMs). The DFMs considered in this work use an unstructured triangular grid to capture the complexity of the fractured porous media. The flow simulation can be accomplished

using either finite element (Baca et al. 1984; Kim and Deo 2000; Karimi-Fard and Firoozabadi 2001; Juanes et al. 2002) or finite volume methods (Granet et al. 2001; Karimi-Fard et al. 2004). Matthäi et al. (2007) presented a method that involves both finite element and finite volume components.

In this work we apply the method of Karimi-Fard et al. (2004). The key advantages of this method are that any type of polygon or polyhedron can be used for gridding and that the method can be applied with any reservoir simulator (such as GPRS) that is based on general connectivity lists. In fact, this procedure has been used in conjunction with GPRS in several previous studies (e.g., Karimi-Fard et al. 2004, 2006). Procedures for upscaling DFMs to coarser representations include the methods of Gong et al. (2006), Karimi-Fard et al. (2006), and Vitel (2007).

The papers addressing naturally fractured reservoirs noted above deal only with the forward flow simulation part of the problem. Attempts to history match NFRs have also been presented in the literature. A composite model that considered an inner high permeability zone and an oil filled outer lower permeability zone was used to history match a fractured reservoir (Smith and Tan 1993). Gang and Kelkar (2006) proposed adjusting the fracture permeability instead of the grid block effective permeability during the history matching. Other approaches have used fracture intensity as a history matching parameter (Suzuki 2004; Cui and Kelkar 2005), where the effective permeability of a grid block was computed from the fracture intensity. A similar method in which cell properties were computed based on the number of fractures that cross each cell was presented by Hu and Jenni (2005). In their work, they proposed a

generalization of the gradual deformation method for history matching object-based models. The method was applied to a fracture network, where fractures were modeled using an object-based approach (Cacas et al. 2001). The history matching was conducted by moving the fracture location along trajectories defined by an algorithm for migrating general Poisson point patterns. Dual-media approaches have also been used with the gradual deformation technique for history matching fractured reservoirs (Jenni et al. 2004).

1.3 Objectives of this work

In general, the history matching of fractured reservoirs represented using DFMs is not as well developed as is the history matching of pixel-based models. For example, the KPCA history matching method (Sarma et al. 2007) has been shown to be accurate and efficient, but its implementation requires the use of pixel-based models, which cannot efficiently capture the complexity of a fractured network. The objective of this thesis is to develop a prototype workflow for history matching naturally fractured reservoirs that combines the efficiency of gradient-based KPCA history matching and the accuracy of flow modeling using DFMs.

The workflow that we present consists of a two-step approach. The first step entails the calibration of a pixel-based model to its equivalent DFM. The calibration parameters consist of a set of coefficients used to determine the grid block permeability and porosity for pixel-based models. The second step consists of

applying the KPCA history matching method to pixel-based images, where grid block permeabilities and porosities are assigned to each block using the calibration established in the first step.

The method as proposed above relies on the existence of a correspondence in flow response between the pixel-based model and its equivalent DFM. The equivalent DFM for a pixel-based model can be obtained by extracting the fracture features in the "pixelized" image of continuous values. Image processing algorithms that perform morphological operations on digitized images, such as the medial axis analysis introduced by Lindquist et al. (1996), can be used to detect the fracture features. In this study we develop an algorithm that uses a "skeletonization" technique to obtain the matrix and fracture elements for the DFM.

This thesis proceeds as follows. In Chapter 2, we demonstrate the application of the KPCA history matching technique to pixel models containing fracture-like features. We then develop and test our procedure for assigning grid block properties to the pixelized models. This property assignment is based on calibration against the underlying DFM. Both of the techniques discussed in this chapter are shown to perform well when run as standalone procedures with two-dimensional models. In Chapter 3, we describe the overall prototype workflow (which combines the two procedures discussed in Chapter 2) and apply it to several two-dimensional model problems. There we demonstrate that the overall procedure is somewhat (though not entirely) effective and that there are still important issues that must be addressed

before the technique can be advocated as a viable procedure for history matching fractured reservoir models. These issues are discussed further in Chapter 4.

Chapter 2

2. History Matching of Fractured Reservoirs

In this chapter, we present each of the individual procedures required for the history matching workflow. The first component entails our approach for flow modeling in naturally fractured reservoirs; in particular we will briefly discuss discrete fracture models (DFMs). The second methodology is the use of kernel principal component analysis (KPCA) as a tool for solving history matching problems. The third component is a calibration step that we propose for linking the pixel models used for the KPCA-based history matching procedure with the DFMs.

2.1 Discrete Fracture Models (DFMs)

For simulations using discrete fracture models, we apply the procedure developed by Karimi-Fard et al. (2004). This approach entails representing individually each fracture for flow simulation purposes, hence capturing accurately the complexity of the fractured reservoir characterization. The accurate representation of each individual

fracture requires the use of unstructured grids. After generating the grid, the next step consists of computing the connectivity list which defines neighboring control volumes. Pore volumes and the transmissibility for each connection are then calculated. These values can then be used with any connection list-based reservoir simulator such as GPRS (Cao 2002).

Since each of the fractures is explicitly represented in the flow simulation model, DFMs can give accurate simulation results. Some numerical inaccuracy may result from the use of two-point flux approximation, but this can be reduced by applying grid optimization techniques. In addition, DFMs can be upscaled using the multiple subregion (MSR) procedure proposed by Karimi-Fard et al. (2006) and later generalized by Gong et al. (2006). These MSR models require much less computational time for flow simulation than do the underlying DFMs.

Although DFMs have several advantages, they cannot be used directly with standard history matching techniques. Figure 2-1, taken from Karimi-Fard et al. (2004), shows a simplified model of a fault zone (upper) and its corresponding DFM (lower). If in the course of history matching fractures are added, moved or deleted, the model must be re-gridded. As discussed earlier, most existing pixel-based history matching techniques apply a fixed grid, so frequent re-gridding would be problematic.

Our goal in this work is to obtain DFMs that match historical production data, so we will need to develop a new history matching procedure.

2.2 History Matching Using KPCA

2.2.1 History matching using PCA

This section reviews the procedure for history matching reservoirs using kernel principal component analysis (KPCA) as proposed by Sarma et al. (2007, 2008). The description here closely follows these earlier developments.

The history matching problem can be seen as an optimization problem in which we adjust the reservoir model, designated **m**, such that the simulated production using this model, $P_{\text{sim}}(\mathbf{m})$, matches the observed production, P_{obs}. Following Sarma et al. (2007) this optimization problem can be represented mathematically as follows:

$$
\begin{aligned}
&\min_{\mathbf{m}} \left[S = \sum_{n=0}^{N-1} \left\{ P_{\text{sim}}^{\text{n}}(\mathbf{x}^{n+1}, \mathbf{m}) - P_{\text{obs}}^{\text{n}} \right\}^2 \right] \\
&\text{subject to} \\
&g^n(\mathbf{x}^{n+1}, \mathbf{x}^n, \mathbf{m}) = 0 \qquad \forall n \in (0, \ldots, N-1) \qquad (2.1) \\
&\mathbf{x}^0 = \mathbf{x}_0 \qquad \text{(initial condition)} \\
&\mathbf{m} \in \text{ geologically consistent realizations}
\end{aligned}
$$

Here, the set of equations $g^n(\mathbf{x}^{n+1}, \mathbf{x}^n, \mathbf{m}) = 0$, with the initial condition $\mathbf{x}^0 = \mathbf{x}_0$, refers to the flow simulation equations that describe (constrain) the dynamic states **x**. The last constraint in Equation 2.1 ensures that the resulting reservoir model **m** is consistent with the geological description.

An efficient way to obtain a model **m** that maintains a degree of geological realism is to apply the Karhunen-Loeve (K-L) or PCA expansion (Oliver 1996; Reynolds et al. 1996; Sarma et al. 2006). This allows us to represent a random field with explicitly known covariance **C** as a series expansion with orthogonal deterministic basis functions, $\mathbf{\Phi}_i$, and uncorrelated random coefficients, ξ_i:

$$\mathbf{m} = \overline{\mathbf{m}} + \xi_1\mathbf{\Phi}_1 + \xi_2\mathbf{\Phi}_2 + \ldots + \xi_l\mathbf{\Phi}_l \tag{2.2}$$

Here $\overline{\mathbf{m}}$ is the average of the random field. The basis functions $\mathbf{\Phi}_i$ are obtained from an eigen-decomposition of the covariance matrix **C** of the random field. As described by Sarma et al. (2007), a procedure for numerically computing **C** is to use a set of conditioned or unconditioned geostatistical realizations $\mathbf{m}_k$, $k = 1, \cdots, N_R$, where the number of realizations N_R should be large enough to yield a converged covariance matrix **C**. These realizations can be generated using a training image, as shown in Figure 2-2, in conjunction with geostatistical algorithms (Strebelle and Journel 2001; Zhang et al. 2006). Using the set of realizations the covariance matrix can be calculated as

$$\mathbf{C} = \frac{1}{N_R}\sum_{j=1}^{N_R}\left[\mathbf{m}_j - \overline{\mathbf{m}}\right]\left[\mathbf{m}_j - \overline{\mathbf{m}}\right]^T \tag{2.3}$$

Here the matrix **C** is of size $N_C \times N_C$, where N_C is the number of cells in the model. A standard algorithm such as singular value decomposition (SVD) could be used to solve the eigenvalue problem

$$\lambda_i \mathbf{v}_i = \mathbf{C}\mathbf{v}_i, \qquad i = 1, \ldots, N_C \tag{2.4}$$

SVD can also work directly with the data matrix (whose columns are $\mathbf{m}_j - \overline{\mathbf{m}}$) rather than with **C**. In Equation 2.2, only l basis functions are retained instead of N_C. These basis functions correspond to the largest of the N_C eigenvalues. The l basis functions are fixed, but by selecting a new set of random coefficients ξ_i, $i = 1, \ldots, l$, we can generate a new realization **m**. The random coefficients are drawn from the standard Gaussian distribution. The expansion as presented above can be very efficient because the parameter space of the model is reduced considerably. Specifically, if the model has N_C cells, only l random coefficients would be required to generate such a model, where l is generally much smaller than N_C.

Sarma et al. (2007, 2008) describe a procedure for determining the $\mathbf{\Phi}_i$ that entails an eigen-decomposition of an $N_R \times N_R$ matrix rater than an eigen-decomposition of **C**, which is $N_C \times N_C$. This technique is discussed below.

2.2.2 Use of KPCA

The principal component analysis (PCA) as presented above only provides a second-moment characterization (two-point spatial statistics) of the geology. In order to capture higher-order statistics, Sarma et al. (2008) proposed to perform the Karhunen-Loeve expansion not in the original space of realizations R^{N_C}, but in a high-order space called feature space F. This requires considering an $N_R \times N_R$ matrix **K**, called the

kernel matrix, instead of the covariance matrix **C**. This kernel matrix is defined as (Schölkopf and Smola 2002):

$$\mathbf{K}: \qquad K_{ij} = \left(\tilde{\mathbf{m}}_i \cdot \tilde{\mathbf{m}}_j\right) \tag{2.5}$$

where $\tilde{\mathbf{m}}_i$ refers to a nonlinear mapping of realization *i* into *F*. According to Equation 2.5, each element of the kernel matrix is a dot product of vectors in the feature space. The tilda in the equation indicates the nonlinear mapping of the realizations $\mathbf{m}_k$ into the feature space *F*. It is not necessary to actually apply the explicit mapping of $\mathbf{m}_k$ to calculate the kernel matrix **K**. Instead the dot product in the feature space *F* can be calculated very efficiently through the use of a kernel function k (Schölkopf and Smola 2002):

$$\left(\tilde{\mathbf{m}}_i \cdot \tilde{\mathbf{m}}_j\right) = k(\mathbf{m}_i, \mathbf{m}_j) \tag{2.6}$$

This kernel function $k(\mathbf{m}_i, \mathbf{m}_j)$ computes the dot product in the feature space *F* directly from the elements $\mathbf{m}_k$ without the need to first perform the nonlinear mapping. Schölkopf and Smola (2002) describe various kernel functions. Following Sarma et al. (2008), sums of polynomial kernels are applied here

$$\left(\tilde{\mathbf{m}}_i \cdot \tilde{\mathbf{m}}_j\right) = k(\mathbf{m}_i, \mathbf{m}_j) = \sum_{n=1}^{d} (\mathbf{m}_i \cdot \mathbf{m}_j)^n \tag{2.7}$$

where *d* is the maximum order of the polynomial kernel. For polynomial kernels of order *d*, the covariance matrix in the feature space *F* corresponds to $2d^{\text{th}}$ order

moments or 2*d*-point statistics of the input space R^{N_C}. In other words, for *d*=1, the covariance matrix in the feature space corresponds to two-point statistics of the input space. The above representation technically preserves all the moments up to the $2d^{\text{th}}$ order moment.

After performing the eigen-decomposition of **K**, the resulting K-L expansion gives a model in feature space *F* in terms of a reduced basis and coefficients

$$\tilde{\mathbf{m}} = \xi_1 \tilde{\mathbf{\Phi}}_1 + \xi_2 \tilde{\mathbf{\Phi}}_2 + \ldots + \xi_l \tilde{\mathbf{\Phi}}_l \tag{2.8}$$

where $\tilde{\mathbf{m}}$ and $\tilde{\mathbf{\Phi}}_i$ are the model and the basis functions respectively in the feature space and ξ_i are random coefficients. This representation needs to be back transformed to the original space to provide physical realizations. This requires an inverse mapping known as a pre-image problem. Sarma et al. (2008) describe a fixed-point iteration method for solving the nonlinear pre-image problem.

As stated earlier, new realizations can be obtained by drawing a new set of random coefficients from the standard Gaussian distribution. Figure 2-3 shows two realizations from KPCA obtained using two different sets of random coefficients. Observe how the fracture features from the training image are captured to some extent in the realizations. KPCA provides continuous (not binary) realizations so the representation is clearly approximate. The pixel values shown in these two realizations can be related to effective block properties (porosity and permeability) for use in the flow simulator.

For instance, high values shown in red in these realizations are related to high values of permeability. This linkage will be quantified later in this chapter.

Now that we have shown how to generate geologically reasonable models with KPCA, we can revisit Equation 2.1 and write the history matching problem as

$$\begin{aligned} &\min_{\boldsymbol{\xi}}\left[S = \sum_{n=0}^{N-1} \left\{ P_{\text{sim}}^{\text{n}}(\mathbf{x}^{n+1}, \boldsymbol{\xi}) - P_{\text{obs}}^{\text{n}} \right\}^2 \right] \\ &\text{subject to} \\ &g^n(\mathbf{x}^{n+1}, \mathbf{x}^n, \boldsymbol{\xi}) = 0 \qquad \forall n \in (0,\ldots,N-1) \\ &\mathbf{x}^0 = \mathbf{x}_0 \qquad \text{(initial condition)} \end{aligned} \tag{2.9}$$

From this equation, we see that the history matching problem now involves finding the set of coefficients $\xi_i, i = 1,\ldots,l$ that minimizes the objective function *S*.

The flow equations in the simulator do not involve $\boldsymbol{\xi}$ directly but rather involve k_x, k_y and ϕ, the permeability components and porosity (in this work we consider only two-dimensional models; for three-dimensional models k_z would also appear). By using the chain rule, we can obtain the gradient of the objective function *S* with respect to $\boldsymbol{\xi}$ as follows

$$\nabla_{\xi} S(\boldsymbol{\xi}) = \frac{\partial S}{\partial k_x}\frac{\partial k_x}{\partial \boldsymbol{\xi}} + \frac{\partial S}{\partial k_y}\frac{\partial k_y}{\partial \boldsymbol{\xi}} + \frac{\partial S}{\partial \phi}\frac{\partial \phi}{\partial \boldsymbol{\xi}} \tag{2.10}$$

Here, the derivatives of the objective function with respect to permeability and porosity can be computed by taking advantage of the adjoint method which is already

implemented in GPRS (see Sarma et al. 2007). The use of adjoints for computing these derivatives is computationally very efficient.

To compute $\partial k_x/\partial \boldsymbol{\xi}$, $\partial k_y/\partial \boldsymbol{\xi}$, and $\partial \phi/\partial \boldsymbol{\xi}$ we apply a numerical perturbation procedure. The numerical perturbation is possible because permeability and porosity are related deterministically to the set of coefficients $\boldsymbol{\xi}$ through functional forms presented below. Conceptually, these functionalities can be represented as

$$\begin{aligned} k_x &= f_1(\psi(\boldsymbol{\xi})) \\ k_y &= f_2(\psi(\boldsymbol{\xi})) \\ \phi &= f_3(\psi(\boldsymbol{\xi})) \end{aligned} \tag{2.11}$$

where ψ represents the pre-image value in a given block resulting from applying KPCA with a given set of coefficients $\boldsymbol{\xi}$. To find the derivative $\partial k_{x,i}/\partial \xi_j$, where $k_{x,i}$ is k_x at block *i* and ξ_j is the j^{th} component of $\boldsymbol{\xi}$, we first find $k_{x,i}$ using Equation 2.11 above. We then apply a small perturbation to ξ_j ($\xi_j = \xi_j + \varepsilon$, where $\varepsilon << 1$) and recompute $k_{x,i}$. This gives a numerical approximation for $\partial k_{x,i}/\partial \xi_j$. We can compute the required gradients for all grid blocks $i = 1, \ldots, N_C$ (and for $\partial k_y/\partial \boldsymbol{\xi}$ and $\partial \phi/\partial \boldsymbol{\xi}$) each time we perturb a component of $\boldsymbol{\xi}$. Computation of these derivatives using numerical perturbation is fast because the number of components of $\boldsymbol{\xi}$ (*l*) is generally small compared to the number of cells (N_C) in the model.

Once the gradient in Equation 2.10 is obtained, the minimization problem of Equation 2.9 can be solved using an appropriate gradient-based algorithm. Here we apply a sequential quadratic programming (SQP) optimization algorithm (Mathworks 2006).

2.2.3 Numerical examples for KPCA history matching

In this section we present two synthetic waterflooding examples demonstrating the application of the KPCA-based history matching approach to fractured reservoir models. Most of the characteristics of these two cases are the same, though they differ in terms of the realization used for the "true" geological model and in the number and location of wells.

The models are two-dimensional and prior geological knowledge is synthesized in the training image presented earlier in Figure 2-2. This training image derives from a very detailed description of an outcrop in the Valley of Fire, Nevada (Flodin and Aydin 2004). The KPCA parameterization of this training image was accomplished using polynomial kernels up to order 2, i.e., d=2 in Equation 2.7, which corresponds to preserving up to four-point statistics of the training image. The parameterization retained the 40 largest eigen-pairs. Two arbitrary sets of random coefficients $\xi_i, i = 1,\ldots,40$ were generated to obtain the "true" geological models (ψ).

The models cover an area of 1600 × 1200 ft^2 (44 acres), are 30 ft in thickness and are represented on grids of dimensions 80 × 60. The top of the reservoir is at 11085 ft and

initial reservoir pressure was set to 5400 psi. Permeability and porosity values were assigned to each grid block by relating the pre-image value (ψ) in each grid block to k_x, k_y and ϕ, as described above (the detailed relationships will be presented in the next section). We consider oil-water systems with strong capillary pressure. Relative permeability curves and capillary pressure curves were taken from experimental data for fractured media (Rangel-German 1999). The oil is of density 0.85 g/cm^3 and viscosity (at initial reservoir conditions) of 0.8 cp.

The models were run for 960 days with both the injectors and producers under bottom hole pressure (BHP) control. Injection pressure was set to 5700 psia and production pressure to 5100 psia. The objective of the history match computations was to estimate the unknown reservoir model (ψ) using observed water injection and oil and water production data.

History matching example 1

This first case involves waterflooding with 3 vertical injectors and 3 vertical producers. The "true" geological model with well locations is shown in Figure 2-4 (top). The quantity actually displayed in this figure is the pre-image value ψ. All of the other characteristics for this case have been described above.

The KPCA-based history matching was done using the initial guess shown in Figure 2-4 (middle). In Figure 2-4 (bottom) we show the reservoir model obtained after the

history matching process. It can be seen that the initial guess model has numerical values of higher magnitude (color intensity) than those of the "true" model. After the KPCA-based history matching, the final model resembles the "true" model reasonably well. Specifically, the magnitudes of the ψ values are in the correct range and the locations of the fracture features and barriers were moved, in many cases, to essentially the correct locations. This is evident in the connections (along fracture features) between Injector 2 and Producer 2 and between Injector 3 and Producer 3. The fracture feature between Injector 1 and Producer 1 does not, however, appear in the history matched model.

Figure 2-5 shows the water injection and oil and water production rates on a field basis. The solid black line corresponds to the injection or production rate for the true model, the dashed red line corresponds to the initial guess, and the dashed blue line is the result for the converged history matched model. It can be seen that the match achieved on the field basis is excellent. The initial model overpredicted both injection and production rates, possibly because it contained ψ values of higher magnitude than those of the "true" model. After the history matching, however, the rates for the matched model closely reproduce the rates of the "true" model.

The match for the individual injectors and producers is also very satisfactory. Figure 2-6 shows the water injection rate for each injector. In this figure, we notice that Injectors 1 and 2 show a very good match. Injector 3 shows slight error, but there is still an improvement from the initial guess. Oil and water production rates for each

producer are shown in Figure 2-7 and Figure 2-8. Each of the producers shows an excellent match in both oil and water production rates.

Figure 2-9 shows the behavior of the objective function with iteration. At the end of the history match, the objective function decreased by almost 3 orders of magnitude. This behavior is consistent with the improvement observed in the injection and production results from the initial guess to the matched model. In all the aspects, the KPCA-based history matching approach performed very well for this example.

History matching example 2

This second case involves waterflooding with 3 injectors and 4 producers. The "true" geological model and the well locations for this example are different than those presented in Example 1. Figure 2-10 (top) shows the "true" geological model and well locations. Other model specifications are the same as in the previous example.

The initial guess used for the KPCA-based history matching of this example is shown in Figure 2-10 (middle). The reservoir model obtained after the history matching process is shown in Figure 2-10 (bottom). Unlike the first example, the initial guess has a narrower range of ψ than does the "true" model. After the KPCA-based history matching, the general magnitude of ψ corresponds reasonably well to that of the "true" model and the history matched model does capture some of the particular characteristics of the "true" model. However, we do not observe visually the level of

agreement in ψ seen in the previous example, and this will be reflected in the flow results.

The water injection and the oil and water production rates for the field are shown in Figure 2-11. As in the first example, the matches at the field level are quite good. The match for field water production shows some error, but improvement from the initial guess is noticeable. The initial model underpredicts injection and production rates, possibly due to the low variability in model properties.

Figure 2-12 shows the water injection rate for each injector. From this figure, we see that the agreement for Injectors 1 and 2 is very close, while slight error is evident for Injector 3. Figure 2-13 and Figure 2-14 show the oil and water production rate respectively for each producer. Here there are much more noticeable discrepancies between results from the history matched and "true" models. In the case of the water production rate for Producer 1, the agreement has actually degraded, though the water rate is very low for this well. For all other production quantities the history matching leads to improvement.

Figure 2-15 shows the behavior of the objective function with iteration. It can be seen that the objective function decreases during the first three iterations and then stalls for the next 10 iterations. At the end of the history match, the objective function has decreased by only about a factor of 20. For this example, the performance of the KPCA-based history matching was acceptable, though clearly not as impressive as in the previous example.

From these and other examples considered, we see that the method performs reasonably well when we represent the fractured reservoir using a pixelized model. This is consistent with the findings of Sarma et al. (2007) who demonstrated accurate history matching results for a variety of geological models. However, our goal is to provide a DFM at the end of the history matching process, so we will need to quantitatively link the history matched pixel model to a DFM.

2.3 Calibration of DFMs

2.3.1 Correspondence between DFM and pixel-based models

In order to obtain a DFM at the end of the history matching process, we must have the ability to "map" between DFMs and pixel (e.g., rectangular grid block) models. We now describe our approach for establishing this linkage.

An appropriate measure of the correspondence between a DFM and a pixelized model can be defined in terms of the mismatch in production responses for the two models. Minimizing this mismatch requires calibrating the pixelized model, in other words finding an optimal transform to obtain permeabilities and porosities from the pre-image values (ψ). Once the correspondence between these two models is established,

then KPCA-based history matching as presented in the previous section can be applied. To better understand the correspondence between DFMs and pixelized models, it is necessary to first describe how each of these models is generated.

In the previous section we described how a pixelized model is generated using KPCA. It basically entails applying Equation 2.2 in the feature space and then solving the pre-image problem to provide the pre-image values. Given a pixelized model, it is possible to obtain the corresponding DFM by performing an image processing step. In this study, we developed an algorithm to process the pixelized image to obtain the fracture segments that define the DFM. Since the pixelized image is continuous, the first step of the algorithm entails generating a binary image by applying a cut-off to the ψ field. The cut-off is taken as the value midway between the two values used to represent fracture and matrix in the geostatistical realizations applied in constructing the KPCA representation. The geostatistical realizations used in this study apply a value of 0 to represent matrix rock and 1 to represent fracture, thus the cut-off applied to the continuous image is 0.5. Figure 2-16 shows the binary image obtained after applying this cut-off to the continuous ψ field. In this binary image we can observe the general orientation and location of the fractures though the image still requires "cleaning" as it includes isolated fracture segments and broken and "smeared" segments.

During the clean up, isolated pixels are removed, broken segments are linked, and the smeared segments undergo a morphological operation. Because we are interested in preserving the shape of the smeared segments (skeleton), we apply a "skeletonization" technique (Mathworks 2006), called medial axis transformation (Haralick 1992; Pratt

2007). The medial axis skeleton obtained consists of the set of points that are equally distant from two closest points of the object (smeared segments) boundary. Figure 2-17 shows the binary image after the “clean up” process.

The segments needed in the DFM are then extracted from the cleaned image. Extracting the segments requires detecting the ends and intersections of the fractures, since straight segments represent the fractures for the DFM. These segments are then input to a mesh generation algorithm (Shewchuk 1996), and a triangular grid is generated for the entire DFM. Figure 2-18 shows a conforming constrained Delaunay triangulation (Shewchuk 1996), where the segments correspond to the fracture control volumes and the triangular cells correspond to the matrix. Physical properties are assigned to each of the control volumes (permeability and thickness for the fractures, permeability and pore volume for the matrix) for the discrete fracture modeling (Karimi-Fard et al. 2004). The final DFM consists of a connectivity list (defining neighboring control volumes) and transmissibilities and pore volumes, which can be used with any connection list-based reservoir simulator such as GPRS (Cao 2002). For our purposes the matrix and fracture permeability and porosity are assumed known (and constant), though in practice these could also be history match parameters. In our case it is only the fracture configuration that is to be determined through history matching.

The calibration is now performed to ensure that the production response of the pixelized model (Figure 2-16, upper) agrees with the production response of its corresponding DFM (Figure 2-18). The properties for the DFM are assumed known so

this model provides the reference or benchmark flow results. The calibration of the pixelized model entails adjusting the parameters used to transform the pre-image values (ψ) into grid block porosities and permeabilities. For this purpose we introduce mappings of the following forms:

$$\begin{aligned} \varphi &= \text{erf}\left[c_1(\psi - c_2)\right] \\ k_x &= c_3 \exp(c_4 \varphi) \\ k_y &= c_5 \exp(c_6 \varphi) \\ \phi &= c_7 + c_8 \varphi \end{aligned} \tag{2.12}$$

The purpose of the error function in the first equation is to bound the φ values used for the determination of k_x, k_y and ϕ. Otherwise extreme (unphysical) values for these quantities could be obtained. The lower bound $\varphi = -1$ corresponds to matrix permeability (i.e., to a block with no fractures). The mapping involves 8 parameters ($c_1 - c_8$) which are adjusted to achieve agreement between the flow response of the pixel-based model and its equivalent DFM. We determine $c_1 - c_8$, designated $\mathbf{c}$, though the following minimization problem

$$\min_{\mathbf{c}} \left[O = \sum_{n=0}^{N-1} \left\{ P^n_{\text{pixel}}(\mathbf{c}) - P^n_{\text{DFM}} \right\}^2 \right] \tag{2.13}$$

where $P_{\text{pixel}}(\mathbf{c})$ is the production resulting from the pixelized model (using the vector $\mathbf{c}$ to map from ψ to grid block properties) and P_{DFM} is the reference production from

the discrete fracture model. The gradient of the objective function with respect to the parameters $\mathbf{c}$ is given by

$$\nabla_{\mathbf{c}} O(\mathbf{c}) = \frac{\partial O}{\partial k_x}\frac{\partial k_x}{\partial \mathbf{c}} + \frac{\partial O}{\partial k_y}\frac{\partial k_y}{\partial \mathbf{c}} + \frac{\partial O}{\partial \phi}\frac{\partial \phi}{\partial \mathbf{c}} \tag{2.14}$$

As described earlier, the derivatives of the objective function with respect to permeability and porosity can be computed efficiently in GPRS using the existing adjoint implementation. The derivatives of porosities and permeabilities with respect to c_1 - c_8 can be determined analytically from Equation 2.12. For completeness the resulting analytical expressions for these derivatives are shown in Equation 2.15. A gradient-based optimization algorithm can be used for the minimization of the objective function in Equation 2.13. Here we applied a sequential quadratic programming algorithm (Mathworks 2006).

$$\begin{aligned}
&\varphi = \operatorname{erf}\left[c_1(\psi - c_2)\right] \\
&\frac{\partial k_x}{\partial c_1} = \frac{2}{\sqrt{\pi}} c_4(\psi - c_2)\, k_x \cdot \exp\left(-\left[c_1(\psi - c_2)\right]^2\right) \\
&\frac{\partial k_x}{\partial c_2} = -\frac{2}{\sqrt{\pi}} c_1 c_4 k_x \cdot \exp\left(-\left[c_1(\psi - c_2)\right]^2\right) \\
&\frac{\partial k_x}{\partial c_3} = \exp(c_4\varphi) \\
&\frac{\partial k_x}{\partial c_4} = k_x\varphi \\
&\frac{\partial k_y}{\partial c_1} = \frac{2}{\sqrt{\pi}} c_6(\psi - c_2)\, k_y \cdot \exp\left(-\left[c_1(\psi - c_2)\right]^2\right) \\
&\frac{\partial k_y}{\partial c_2} = -\frac{2}{\sqrt{\pi}} c_1 c_6 k_y \cdot \exp\left(-\left[c_1(\psi - c_2)\right]^2\right)
\end{aligned}$$

$$
\begin{aligned}
\frac{\partial k_y}{\partial c_5} &= \exp(c_6\varphi) \\
\frac{\partial k_y}{\partial c_6} &= k_y\varphi \\
\frac{\partial \phi}{\partial c_1} &= \frac{2}{\sqrt{\pi}} c_8(\psi - c_2)\cdot \exp\left(-\left[c_1(\psi - c_2)\right]^2\right) \\
\frac{\partial \phi}{\partial c_2} &= -\frac{2}{\sqrt{\pi}} c_1 c_8 \cdot \exp\left(-\left[c_1(\psi - c_2)\right]^2\right) \\
\frac{\partial \phi}{\partial c_7} &= 1 \\
\frac{\partial \phi}{\partial c_8} &= \varphi
\end{aligned}
\qquad (2.15)
$$

2.3.2 Numerical examples demonstrating calibration procedure

The calibration procedure is illustrated with two synthetic waterflooding examples. The two cases are the same except for the number and location of wells.

The models are two-dimensional and the "true" fractured system is represented with the DFM shown in Figure 2-18. This DFM was obtained by performing an image processing step on the pixel-based model of Figure 2-16 (upper). The models cover an area of 1600 × 1200 ft^2 (44 acres), are 30 ft in thickness and are represented on triangulated grids as seen in Figure 2-18. This triangulated grid consists of 254 linear control volumes representing fracture elements and 688 triangular control volumes representing the matrix. Reservoir settings are the same as those defined in the earlier examples; e.g., initial reservoir pressure is 5400 psi. The permeability and aperture of the fractures are 400,000 md and 0.344 mm respectively. The matrix rock is of

permeability 100 md and porosity 30%. Oil and water properties, relative permeabilities and capillary pressures are as in the previous examples.

To obtain the reference production from the DFM, the models were run for 960 days with both the injectors and producers under bottom hole pressure (BHP) control. Injection pressure was set to 5700 psi and production pressure to 5100 psi. The objective of the calibration procedure is to determine the calibration parameters $c_1 - c_8$, necessary to transform the pre-image values (ψ) of the pixel-based model to k_x, k_y and ϕ, such that the production resulting from this pixel-based model agrees with the production from the reference DFM. In the two examples presented here, the initial guess for the calibration parameters corresponds to the set $\mathbf{c}$ that provides the matrix permeability for the lower bound $\varphi = -1$ and a simply computed "effective" permeability of a matrix block containing a fracture for the upper bound $\varphi = +1$. For this calibration procedure, the pixel-based model was represented on a 2D grid of dimensions 80 × 60. Figure 2-16 (upper) shows the pre-image values (ψ) of the pixel-based model.

Calibration example 1

This first case involves waterflooding with 3 injectors and 4 producers. The well locations in the pixel-based model are shown in Figure 2-19 (upper). All of the other characteristics for this case have been described above.

The calibration procedure was performed using the initial guess described above. After the calibration procedure a correspondence – in terms of flow response – between the DFM and the pixel-based model was established. Figure 2-20 shows the water injection and oil and water production rates on a field basis. The solid black line corresponds to the reference injection or production rate for the DFM, the dashed red line corresponds to results using the initial guess for the parameters in the pixel-based model, and the dashed blue line is for the optimized calibration parameters in the pixel-based model. It can be seen that after the calibration, the agreement between the DFM and the pixel-based model is very good. It is evident, however, that the initial guess parameters lead to large discrepancies with the DFM, so it should be possible to establish a better procedure for the initial specification of **c**.

The level of agreement for individual injectors and producers is also quite reasonable. Figure 2-21 shows the water injection rate for each injector. Oil and water production rates for each producer are shown in Figure 2-22 and Figure 2-23. Producer 3 shows the largest discrepancies, though results for this well are still acceptable.

Figure 2-24 shows the behavior of the objective function. It can be seen that the objective function decreases by about four orders of magnitude. This dramatic reduction is due in part to the high degree of inaccuracy of the initial guess. In any event, this example demonstrates that the calibration procedure is able to provide parameters for the pixel model that result in flow predictions that are in close agreement with those from the corresponding DFM.

Calibration example 2

This second case involves waterflooding with 3 injectors and 3 producers. The well locations in the pixel-based model are shown in Figure 2-25. Other problem specifications are as in the previous example.

Figure 2-26 shows the water injection and oil and water production rates on a field basis. The agreement between the DFM and the calibrated pixel-based model is again close. Figure 2-27 shows the water injection rates and Figure 2-28 and Figure 2-29 present the oil and water production rates. Overall, these results again demonstrate that the calibration procedure is able to provide accurate pixel models. The improvement resulting from the calibration procedure is also evident in Figure 2-30 where we show the decrease in the objective function.

From both examples we see that it is possible to represent fractured reservoirs with a pixel-based model provided that a calibration procedure is applied. In the next chapter, we combine the two techniques discussed in this chapter to define an overall history matching procedure.

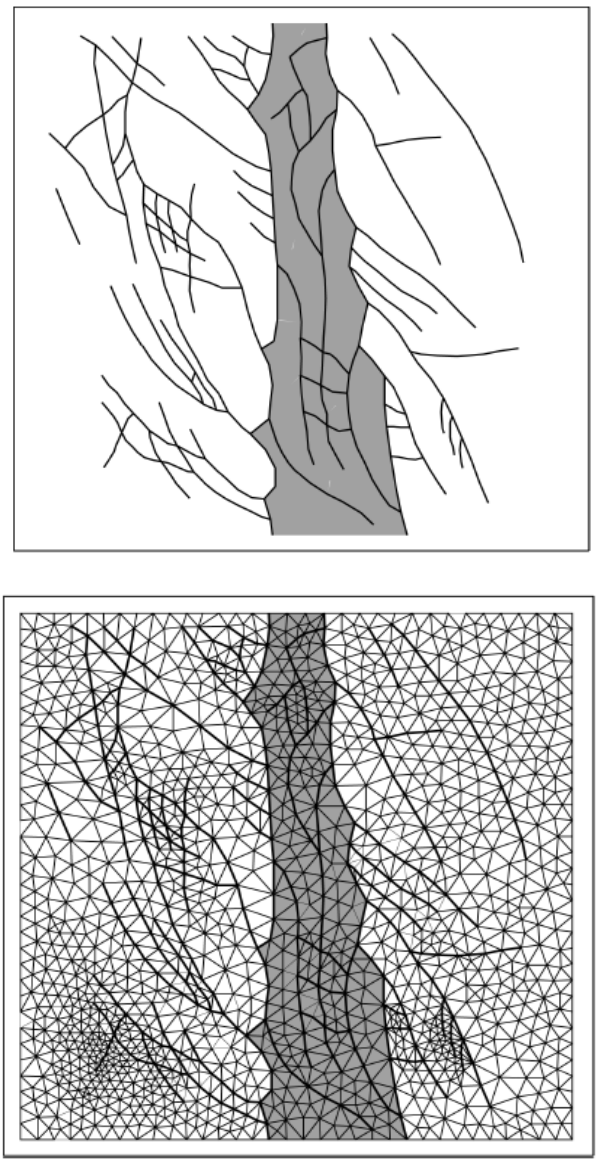

Figure 2-1 DFM for a simplified fault zone (from Karimi-Fard et al. 2004)

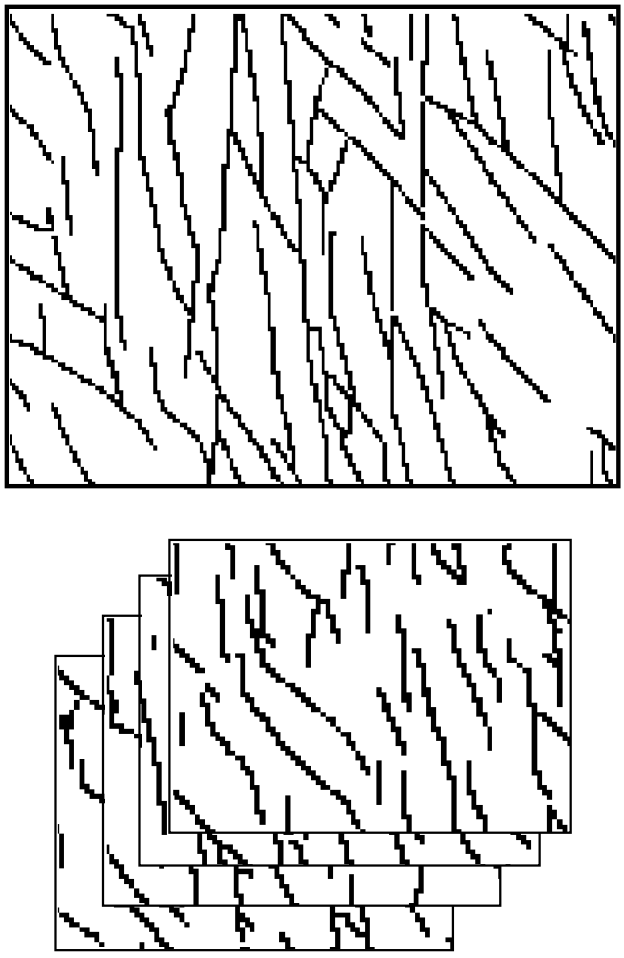

Figure 2-2 Training image for a fractured reservoir (adapted from Flodin and Aydin 2004) and some corresponding geostatistical realizations (lower)

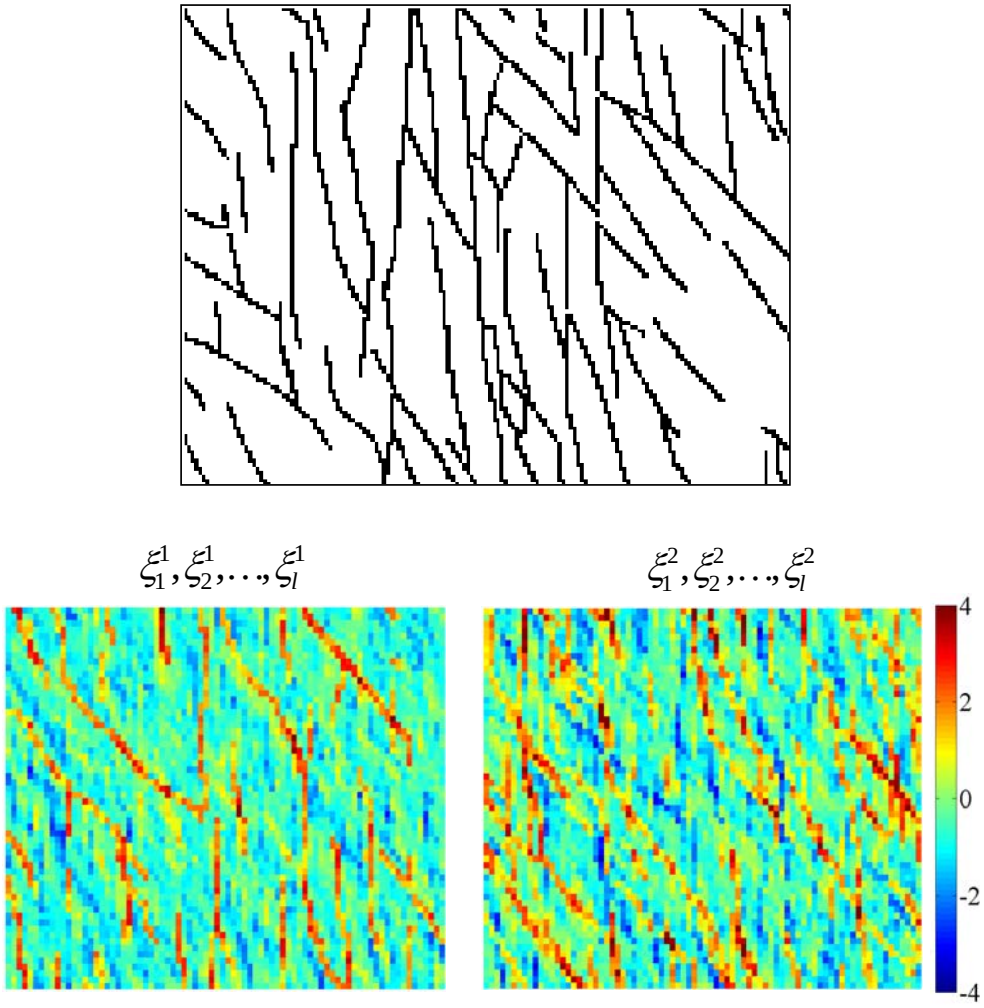

Figure 2-3 Training image and two KPCA realizations generated with two different sets of random coefficients

a) true

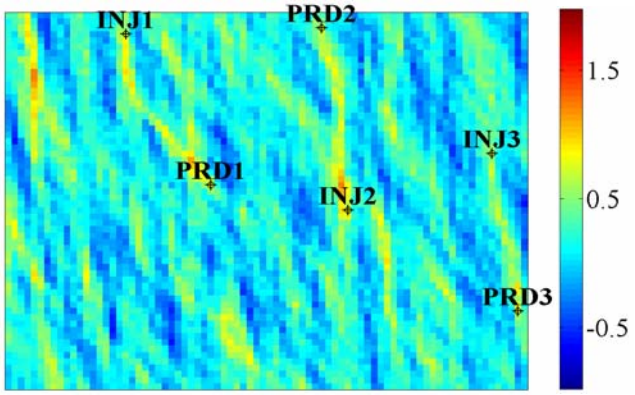

b) initial

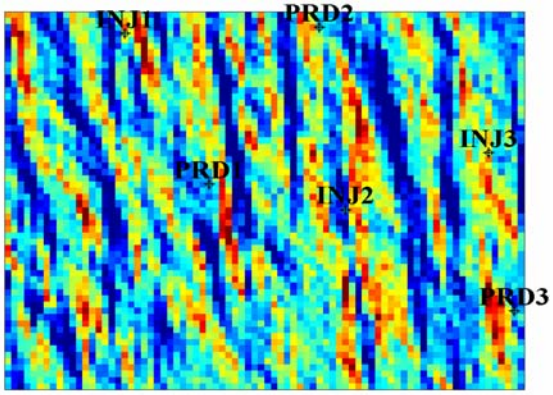

c) matched

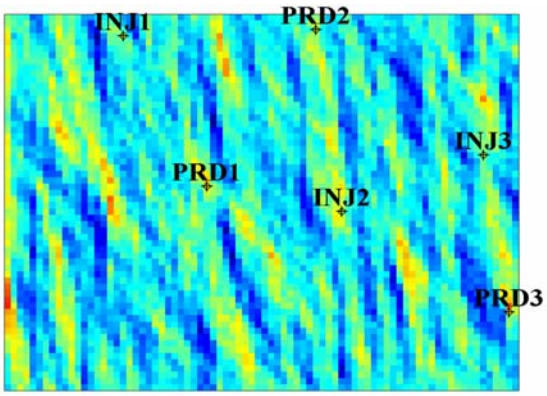

Figure 2-4 True, initial guess and matched model (history matching example 1)

a) field water injection

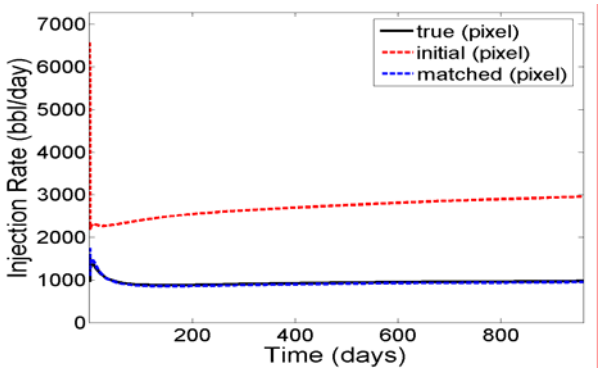

b) field oil production

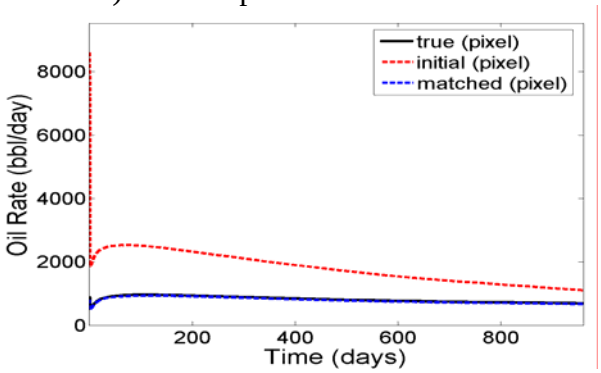

c) field water production

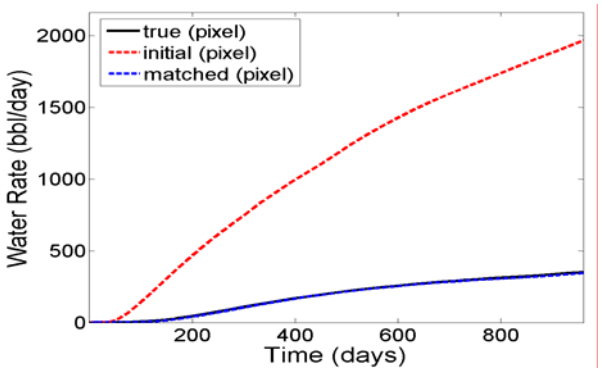

Figure 2-5 Field injecting and producing rates for the true, initial and history matched models (history matching example 1)

a) injector 1

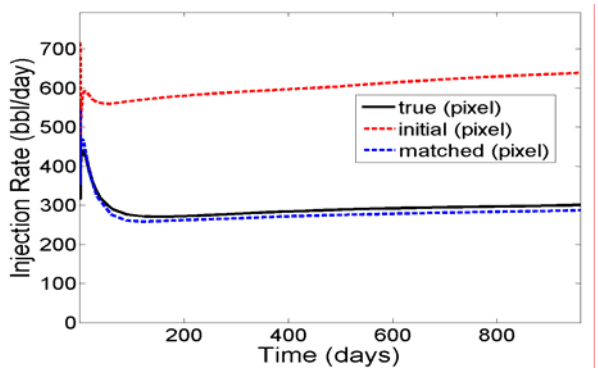

b) injector 2

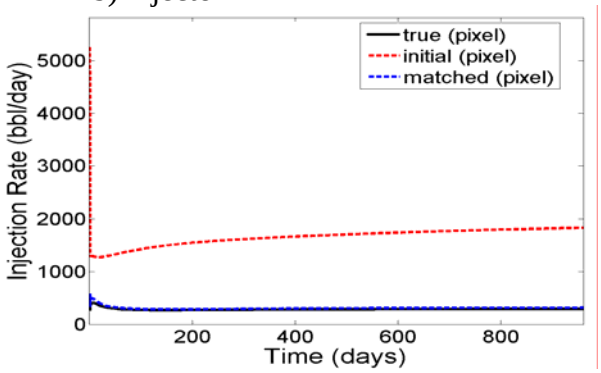

c) injector 3

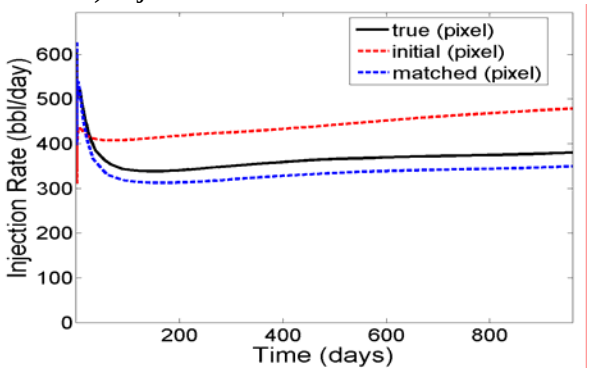

Figure 2-6 Well injection rates for the true, initial and history matched models (history matching example 1)

a) producer 1

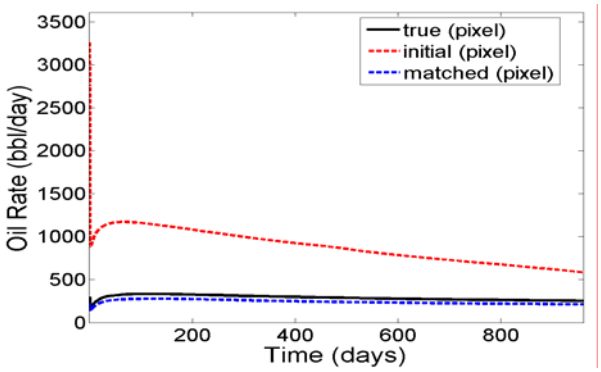

b) producer 2

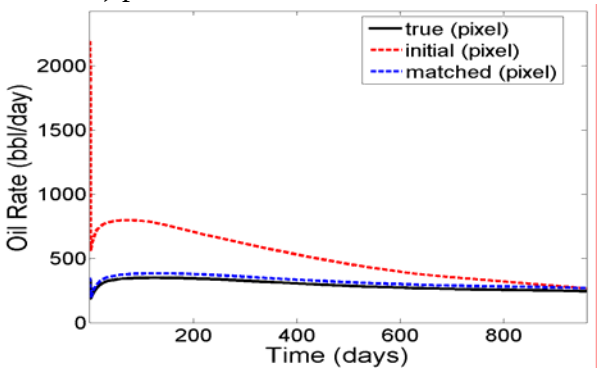

c) producer 3

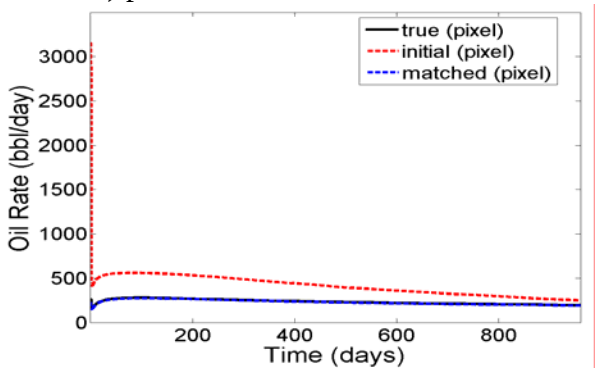

Figure 2-7 Well oil production for the true, initial and history matched models (history matching example 1)

a) producer 1

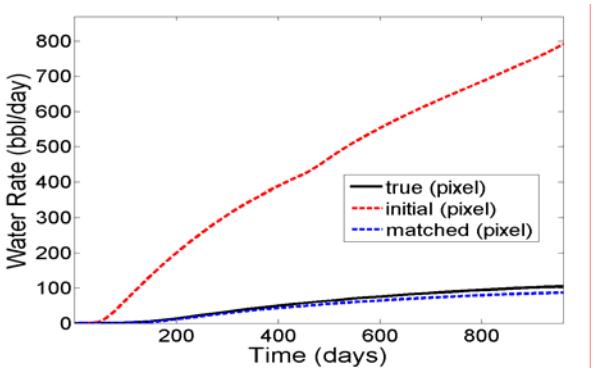

b) producer 2

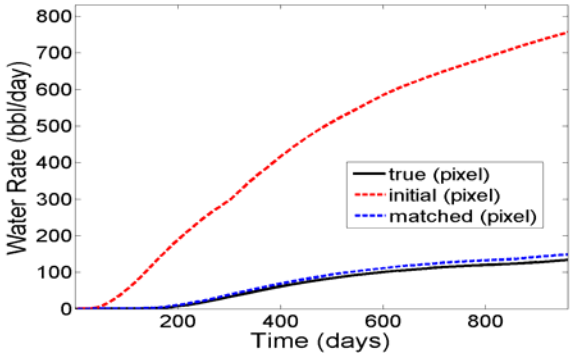

c) producer 3

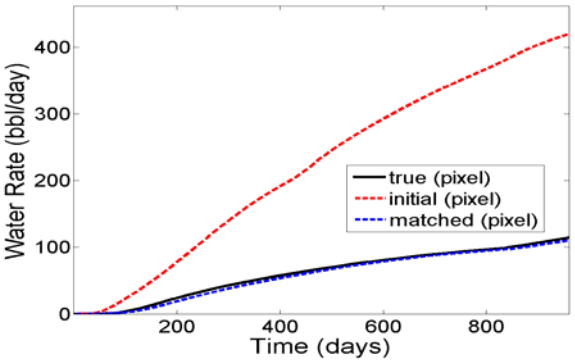

Figure 2-8 Well water production rates for the true, initial and history matched models (history matching example 1)

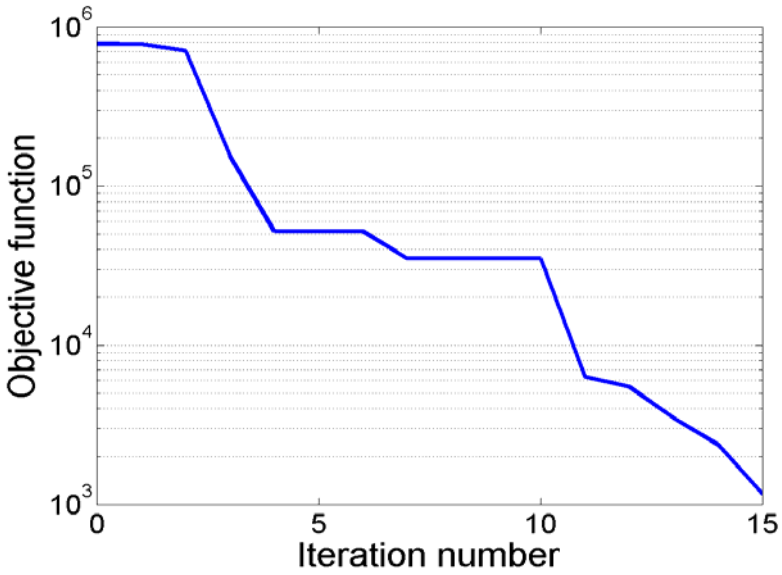

Figure 2-9 Behavior of objective function with iteration number (history matching example 1)

a) true

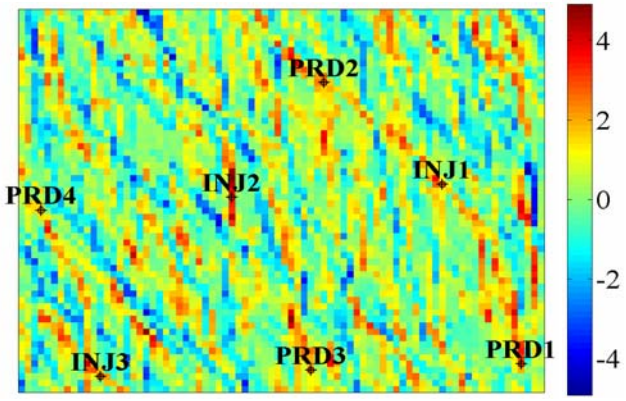

b) initial

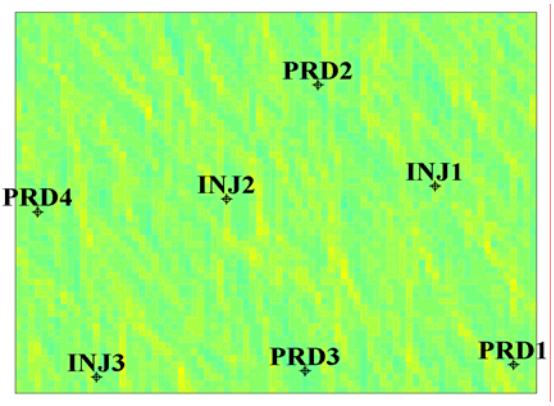

c) matched

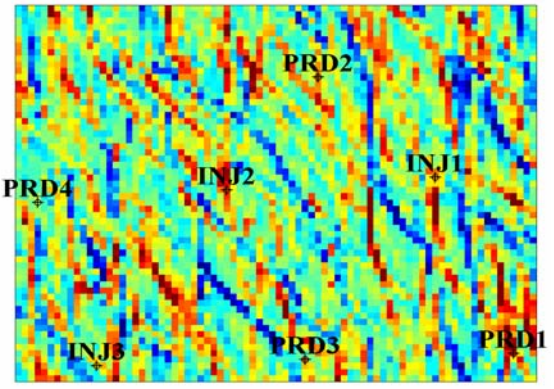

Figure 2-10 True, initial guess and matched model (history matching example 2)

a) field water injection

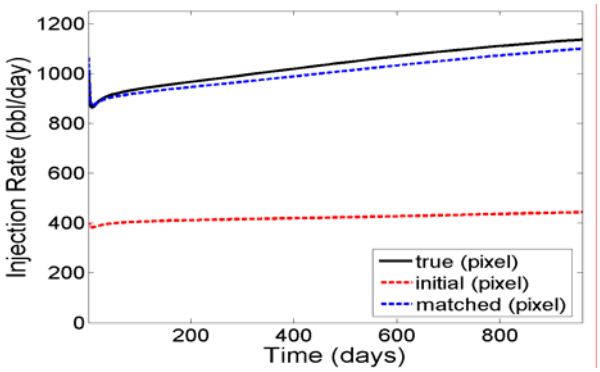

b) field oil production

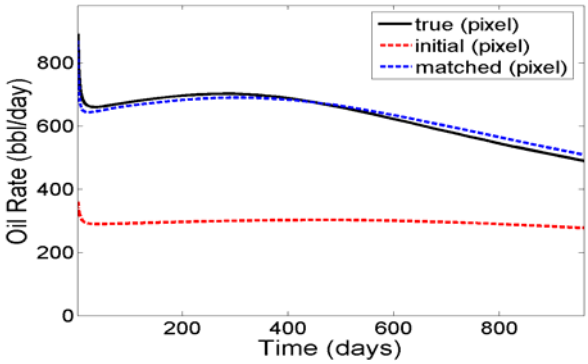

c) field water production

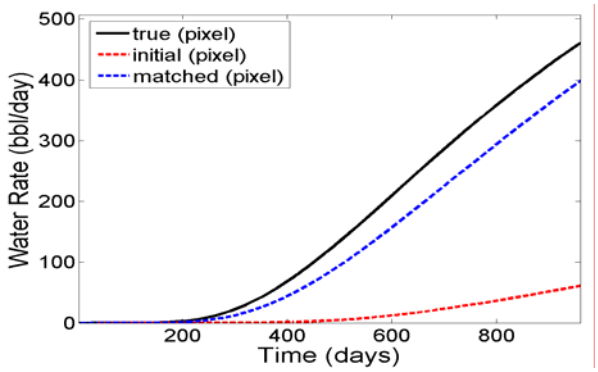

Figure 2-11 Field injecting and producing rates for the true, initial and history matched models (history matching example 2)

a) injector 1

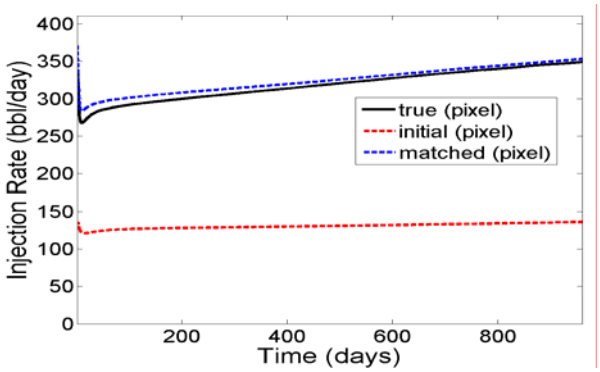

b) injector 2

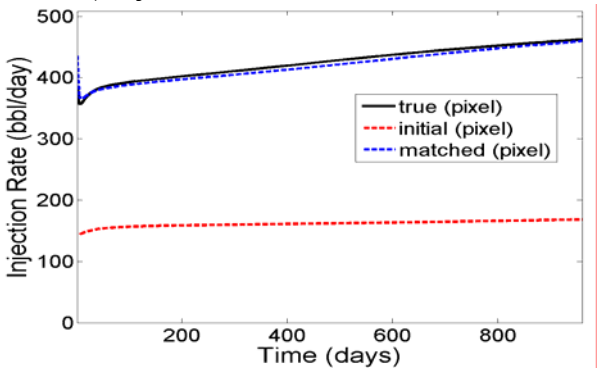

c) injector 3

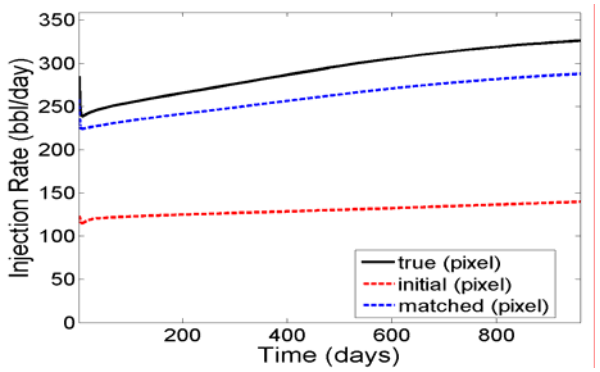

Figure 2-12 Well injection rates for the true, initial and history matched models (history matching example 2)

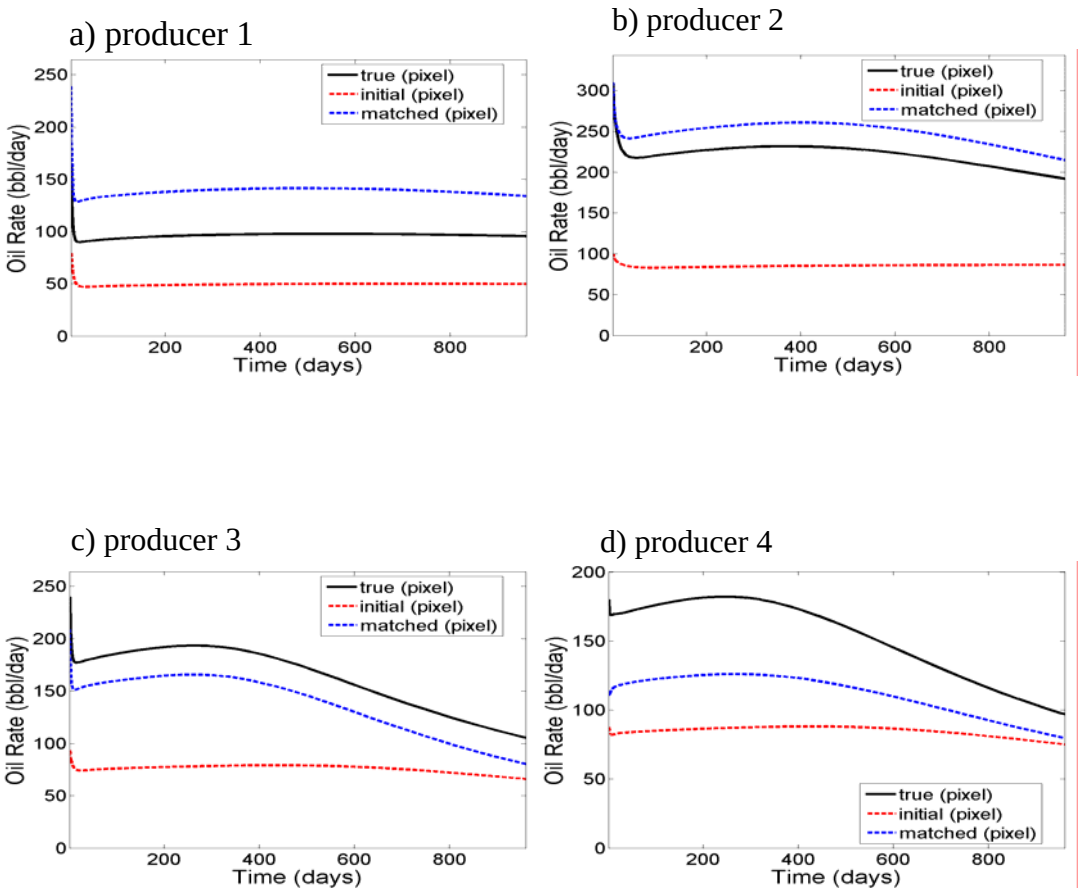

Figure 2-13 Well oil production for the true, initial and history matched models (history matching example 2)

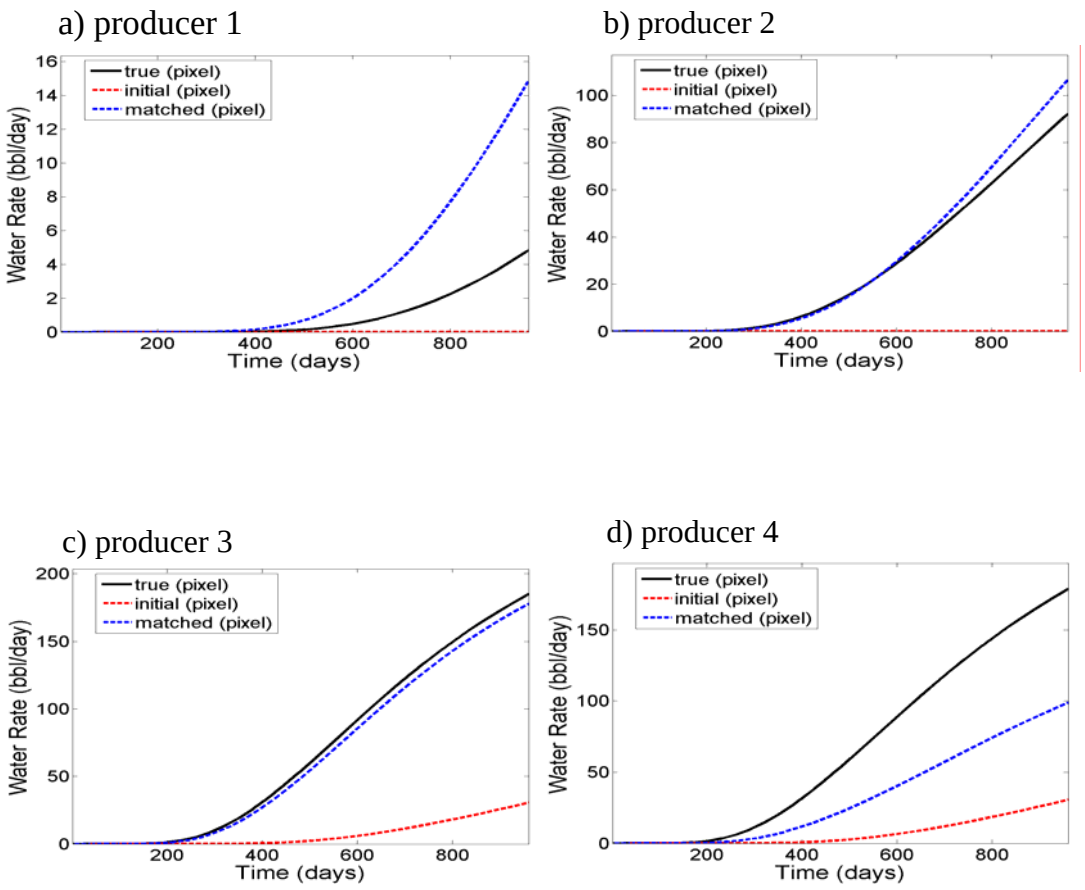

Figure 2-14 Well water production rates for the true, initial and history matched models (history matching example 2)

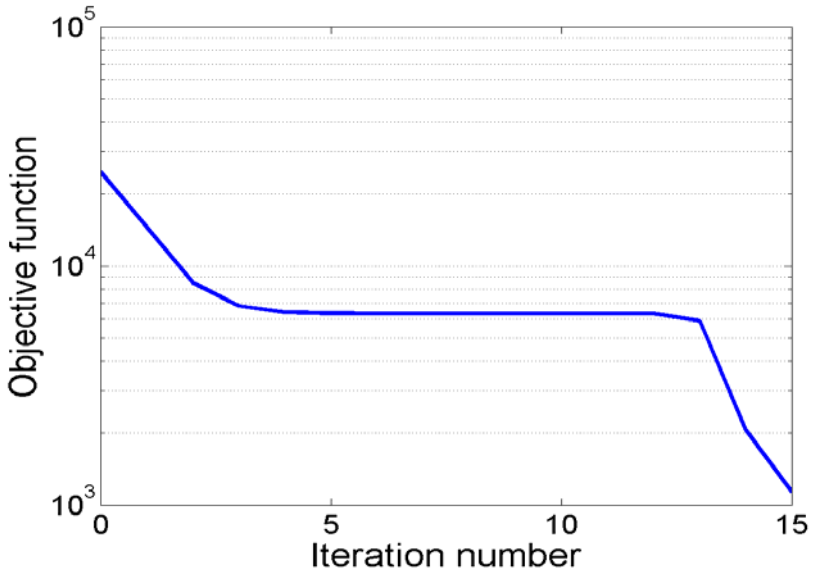

Figure 2-15 Behavior of objective function with iteration number (history matching example 2)

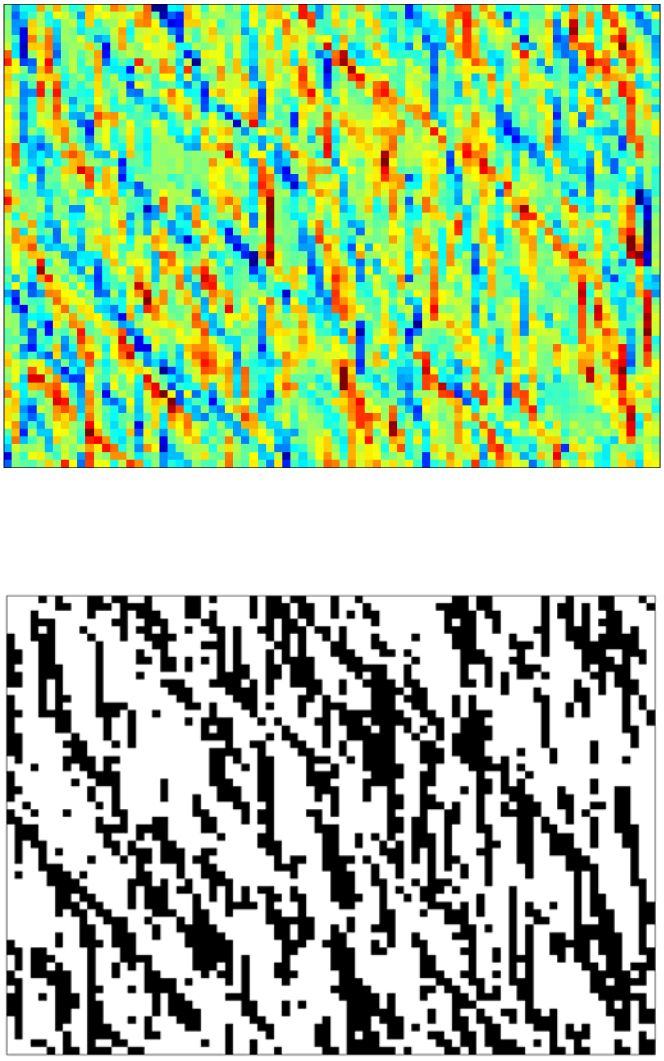

Figure 2-16 Pre-image and equivalent binary image after applying a cut-off

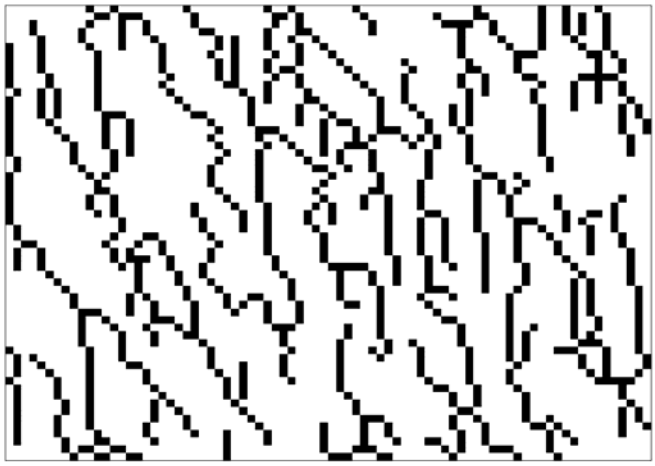

Figure 2-17 Binary image obtained after the clean up process

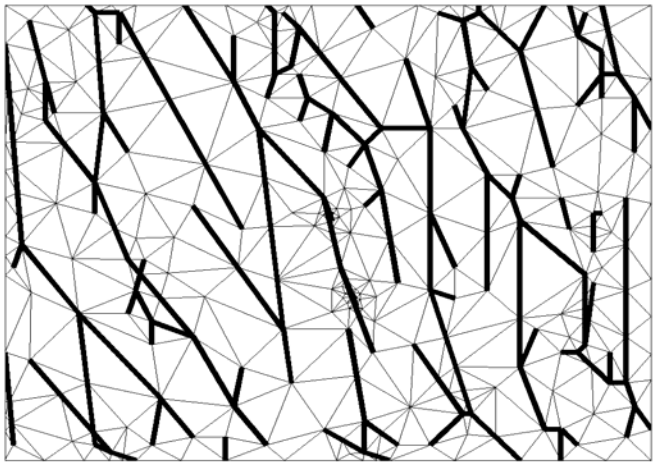

Figure 2-18 Geometrical representation of the DFM

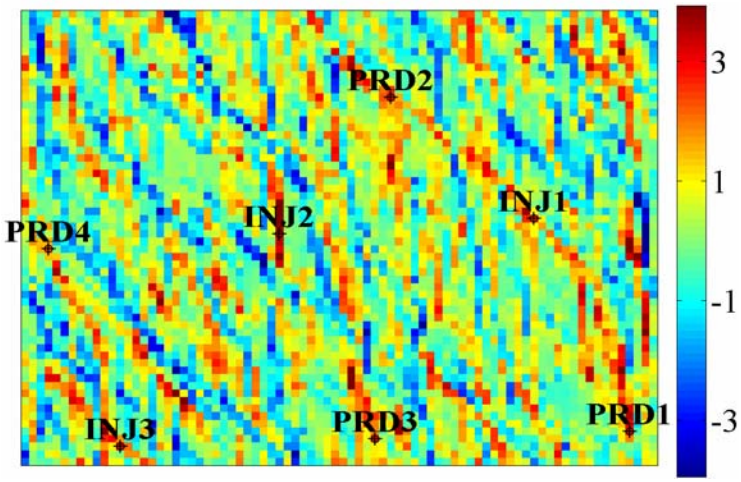

Figure 2-19 Well locations on pixel-based model for calibration example 1

a) field water injection

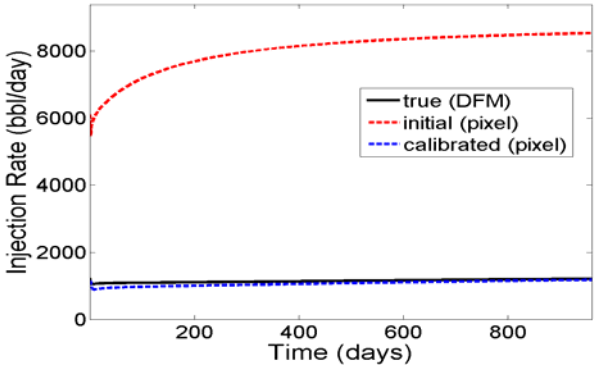

b) field oil production

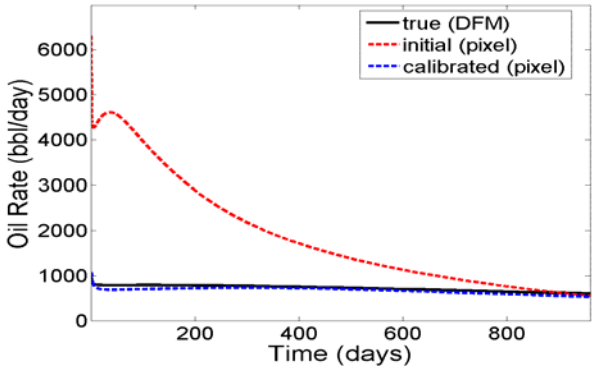

c) field water production

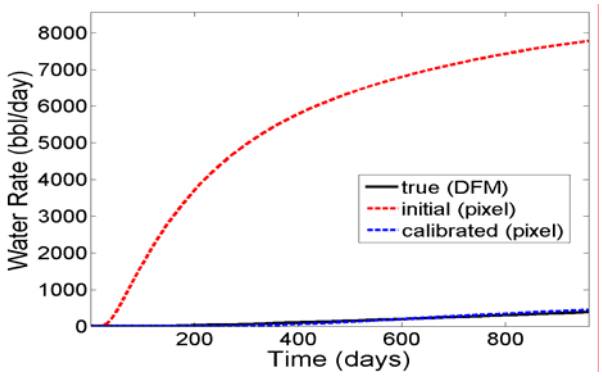

Figure 2-20 Field injection and production rates for the DFM, initial and calibrated model (calibration example 1)

a) injector 1

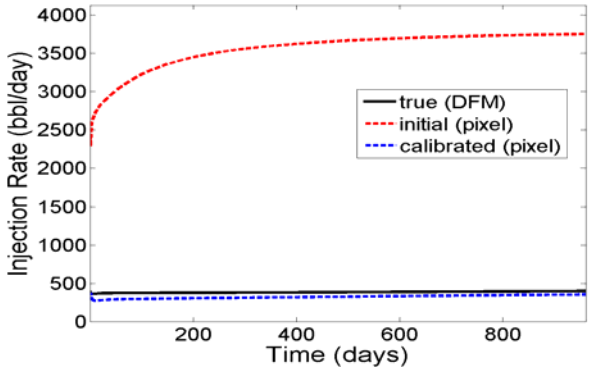

b) injector 2

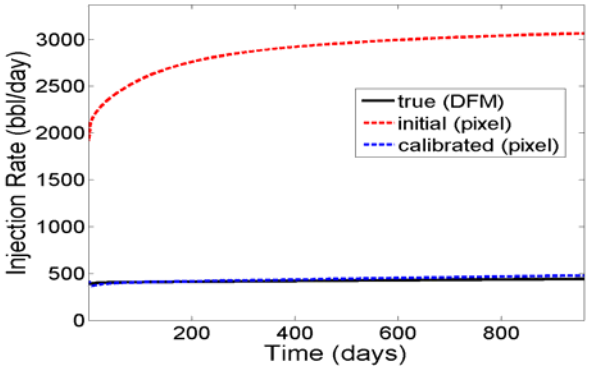

c) injector 3

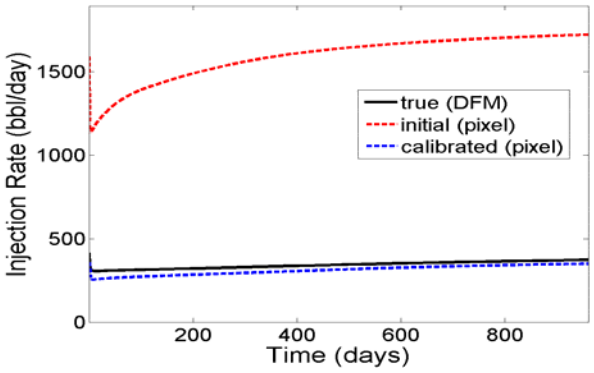

Figure 2-21 Well water injecting rates for the DFM, initial and calibrated models (calibration example 1)

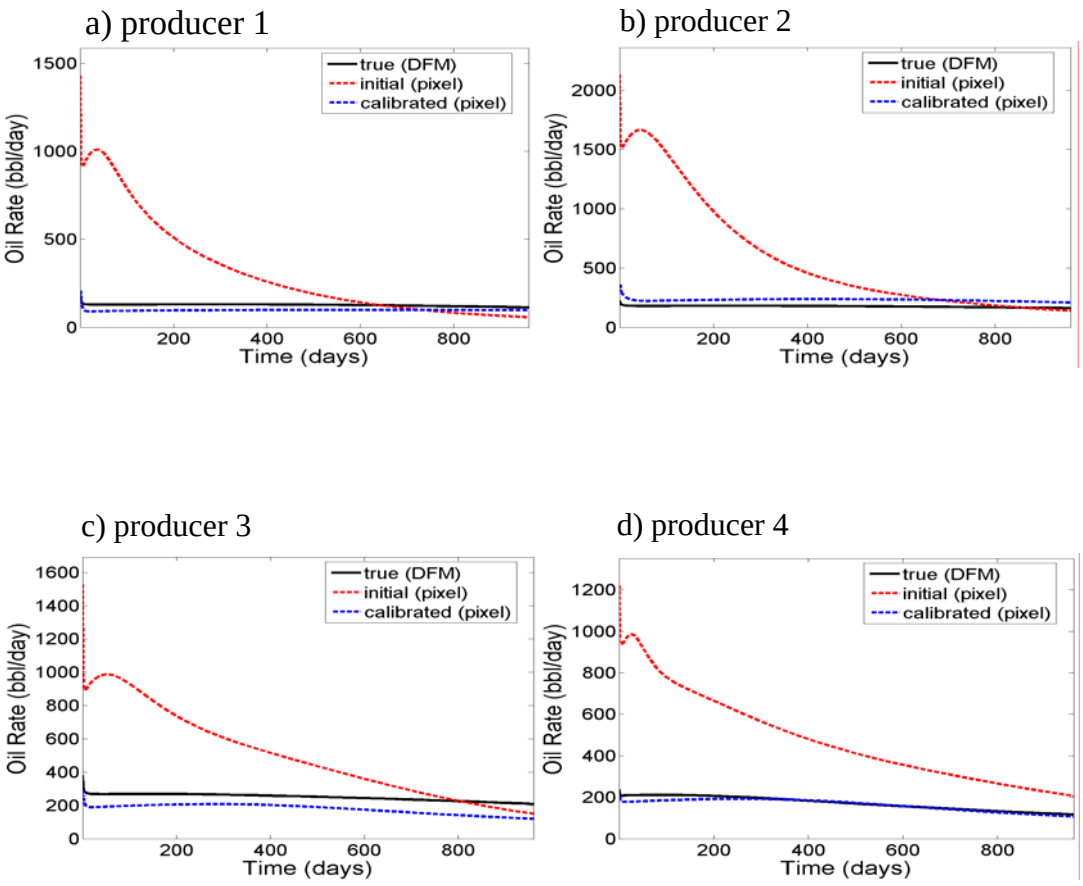

Figure 2-22 Well oil producing rates for the DFM, initial and calibrated models (calibration example 1)

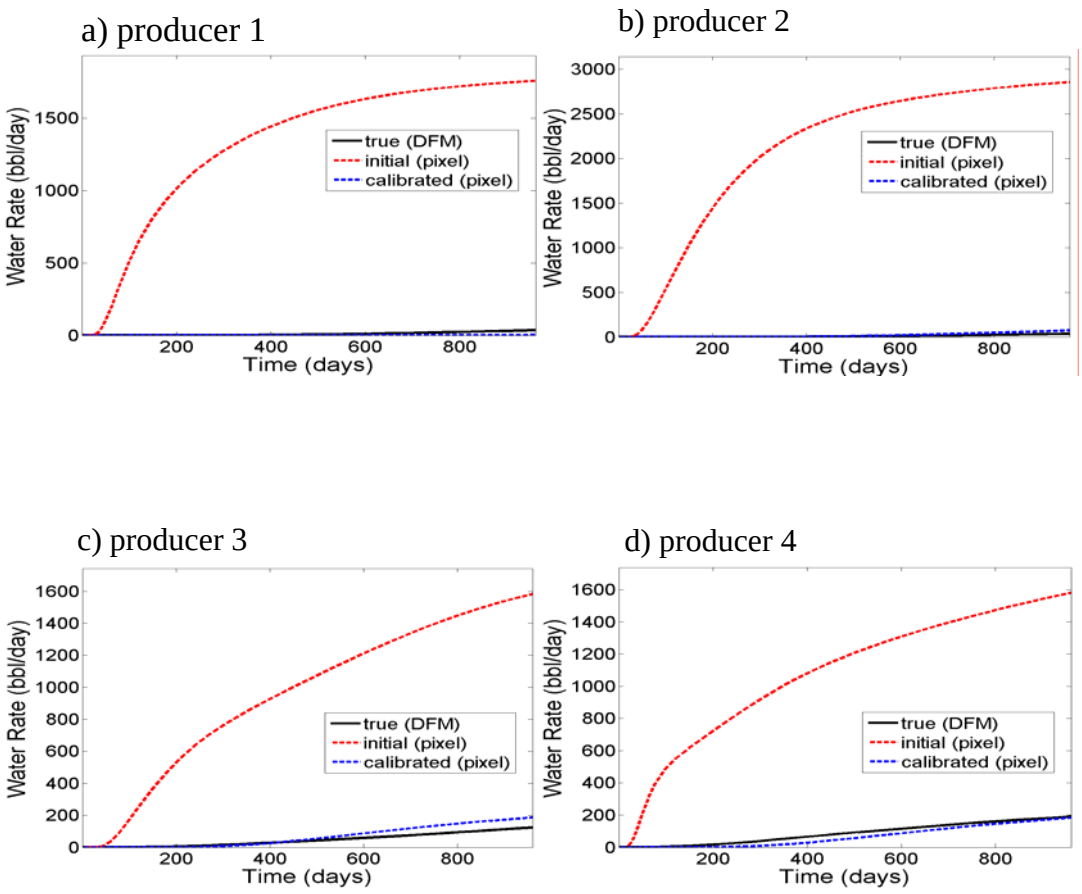

Figure 2-23 Well water producing rates for the DFM, initial and calibrated models (calibration example 1)

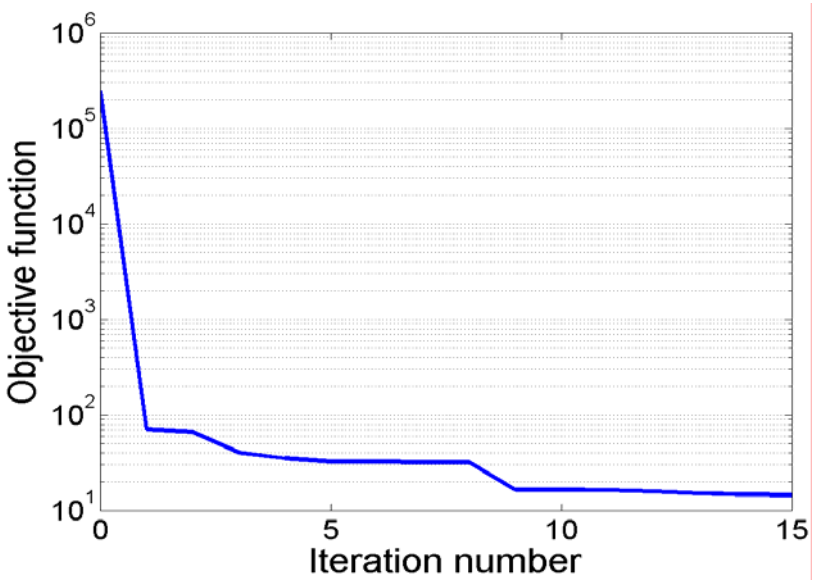

Figure 2-24 Behavior of the objective function during the calibration (calibration example 1)

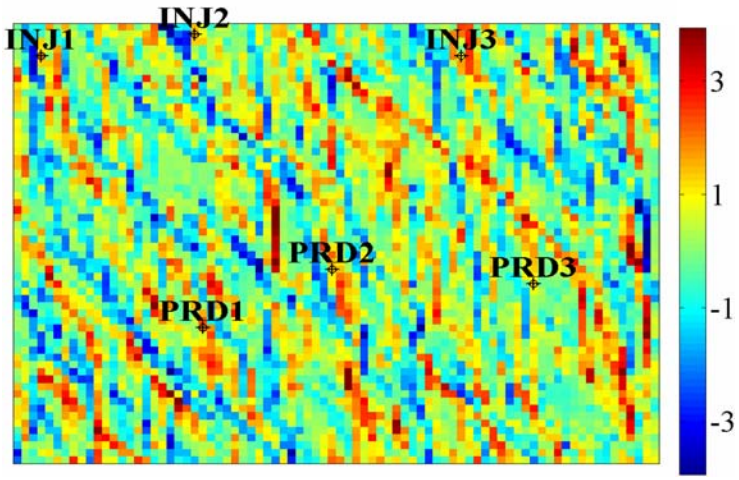

Figure 2-25 Well locations on pixel-based model for calibration example 2

a) field water injection

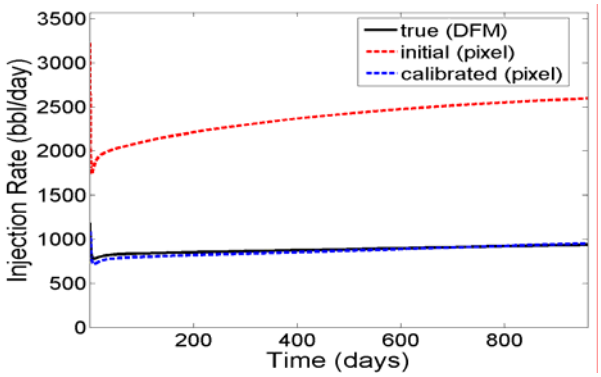

b) field oil production

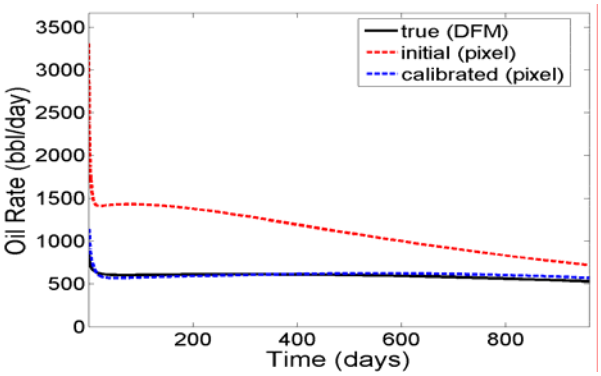

c) field water production

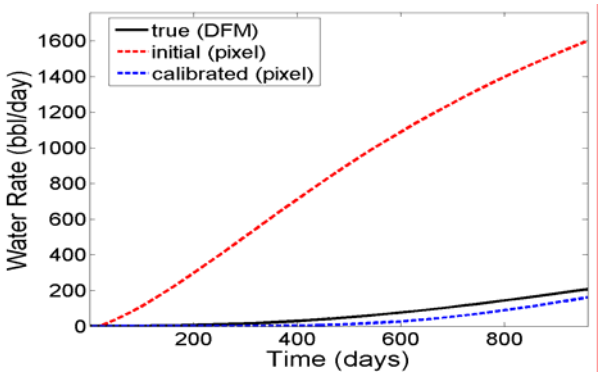

Figure 2-26 Field injection and production rates for the DFM, initial and calibrated model (calibration example 2)

a) injector 1

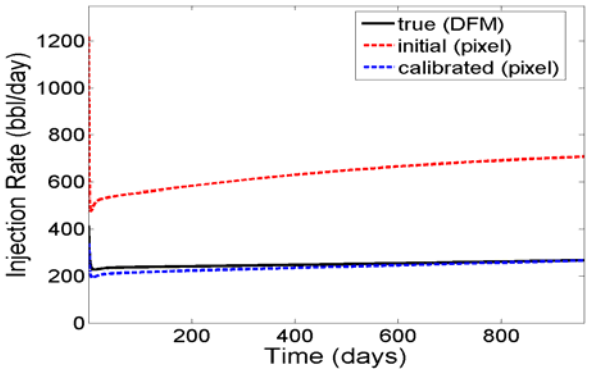

b) injector 2

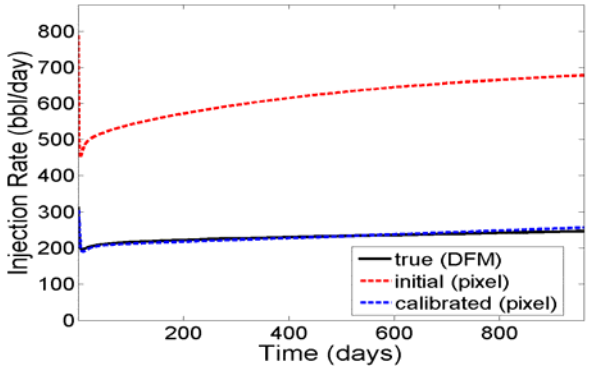

c) injector 3

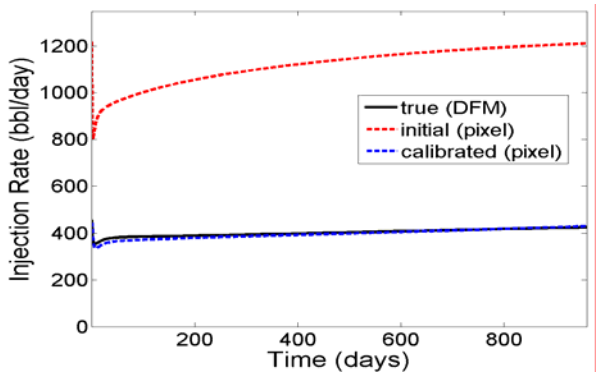

Figure 2-27 Well water injecting rates for the DFM, initial and calibrated models (calibration example 2)

a) producer 1

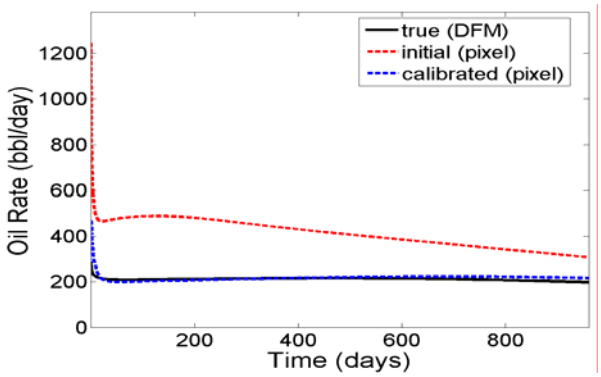

b) producer 2

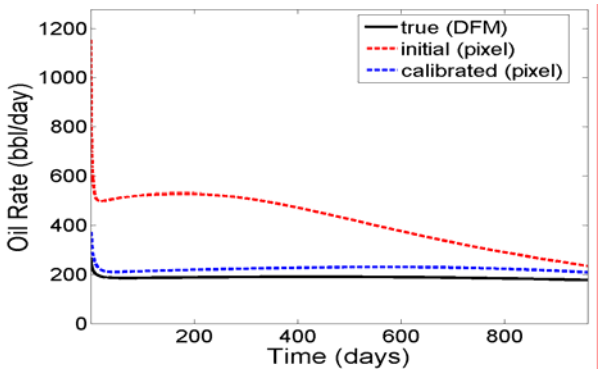

c) producer 3

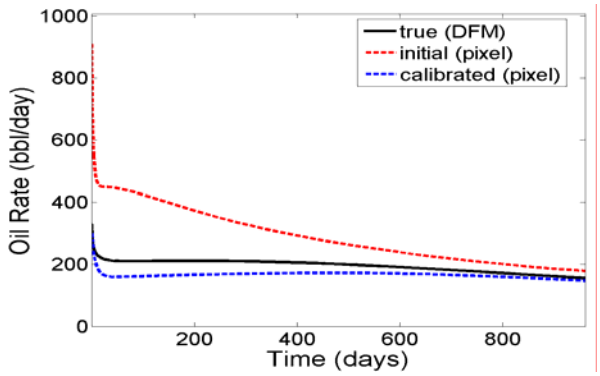

Figure 2-28 Well oil producing rates for the DFM, initial and calibrated models (calibration example 2)

a) producer 1

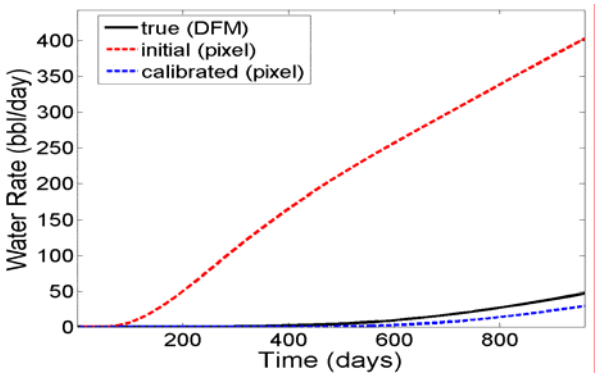

b) producer 2

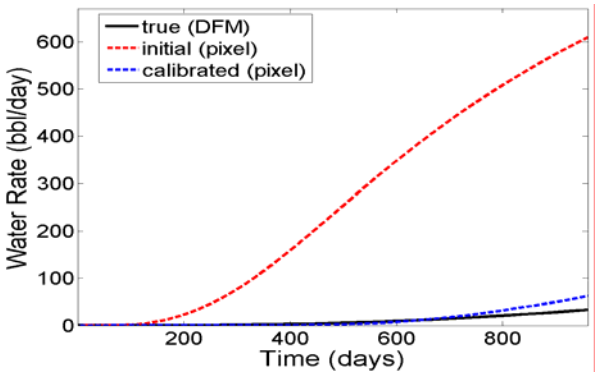

c) producer 3

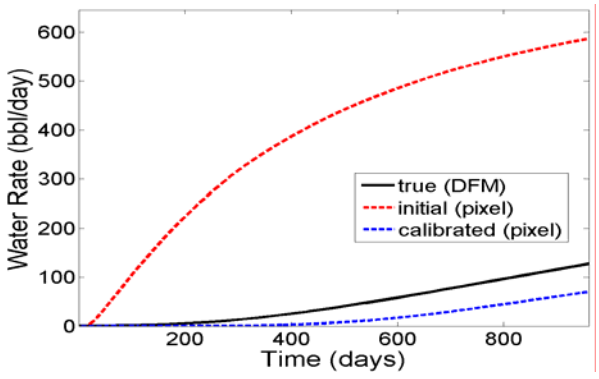

Figure 2-29 Well water producing rates for the DFM, initial and calibrated models (calibration example 2)

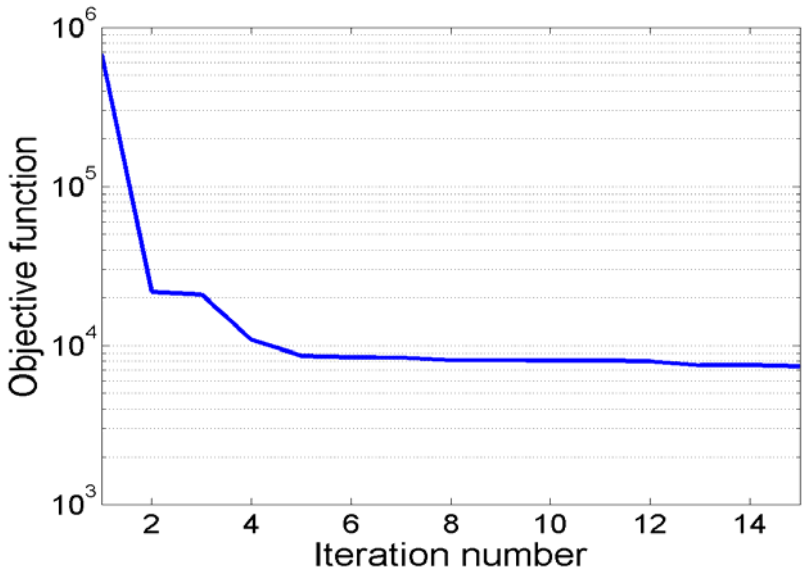

Figure 2-30 Behavior of the objective function during the calibration (calibration example 2)

Chapter 3

3. Workflow for History Matching NFRs

In this chapter, we describe a prototype workflow for history matching two-dimensional fractured reservoirs. The workflow consists largely of the two steps described and validated in Chapter 2. We now describe the overall procedure and then demonstrate its application on three examples.

3.1 Overall history matching workflow

The overall history matching procedure presented here is best viewed as a proof of concept prototype. The results demonstrate that the technique shows promise, though there are aspects of the method that will require refinement before it can be considered for practical use. We now describe the procedure and point out some of the treatments that may need to be reconsidered in future work.

The steps of the workflow are as follows:

1. Develop a training image that characterizes the geological model. Once the training image is established, apply an appropriate multipoint geostatistical

algorithm (e.g., Strebelle and Journel 2001; Zhang et al. 2006) to generate a large number of realizations.

2. Apply the KPCA modeling procedure to provide a reduced basis (consisting of l vectors) that can be used to represent the geological model in feature space (this representation will be in the form of Equation 2.8). A model in physical space can then be generated by constructing the pre-image.
3. Generate the "true" DFM. This is accomplished by selecting random ξ_i, $(i = 1,\ldots,l)$, constructing the pre-image ψ, and then applying the cut-off, skelotonization, and clean-up algorithms described in Section 2.3.1. Properties for the fractured reservoir (e.g., porosities, permeabilities, relative permeability curves, capillary pressures) must also be assigned. Then, simulate the "true" DFM (for particular well locations and well settings) to generate the "true data" to be used in the history match.
4. Establish the calibration that links pixel (i.e., Cartesian) models to discrete fracture models (DFMs). This entails the determination of the coefficients $c_1 - c_8$ in Equation 2.12 that minimize the difference in flow predictions between the DFM and the pixel model. In this work, this calibration is performed using the "true" DFM and the pixel model used to generate this "true" DFM (we refer to the latter model as the "true pixel-based model"). This is in a sense somewhat unfair, as in a real case the "true" model is unknown so the calibration cannot be performed using it. We proceed in this way here, however, as our intent at this point is to demonstrate the general procedure rather than to develop a practical algorithm. Approaches that are more

applicable in practice, involving for example calibration over multiple models and/or occasional updating of the calibration parameters during the course of the optimization, should be investigated in future work.

5. At this point the calibration parameters are established and pixel-based simulations are possible. Thus, we now generate an initial guess pixel model (by selecting random ξ) and then apply the KPCA-based history matching procedure to generate a history matched pixel model.
6. Apply the cut-off, skelotonization, and clean-up algorithms described in Section 2.3.1 to the history matched pixel model to generate a DFM. This "history matched DFM" is the final product of the overall workflow.

Steps 5 and 6 can be repeated using different initial guesses, which will provide multiple history matched models. In addition, the entire procedure can be repeated using different training images to better quantify the effects of reservoir uncertainty. Neither of these options is considered here.

3.2 Numerical examples for the overall workflow

We now present three synthetic waterflooding examples demonstrating the application of the prototype workflow for history matching 2D fractured reservoirs. Example 1 and Example 2 use the same "true" geological model but have different well

configurations. Example 3 involves a different "true" geological model and a different set of wells than the other two examples.

The models are characterized by the same training image used for the examples in Chapter 2 (see Figure 2-2). The KPCA parameterization of this training image was accomplished using polynomial kernels up to order 2. The 40 largest eigen-pairs were retained. As in the examples considered in Chapter 2, the models here cover an area of 1600×1200 ft^2 (44 acres), are 30 ft in thickness, and are at an initial reservoir pressure of 5400 psi. The underlying (DFM) permeability and fracture aperture are 400,000 md and 0.344 mm; matrix rock permeability and porosity are 100 md and 30%. The same oil-water properties are considered here as in the Chapter 2 examples. All models were simulated for 960 days. Injection pressure was again set to 5700 psi and production pressure to 5100 psi. Pixel-based models were in all cases represented on an 80×60 grid; DFMs were represented on an unstructured triangular grid.

Example 1

The first case involves waterflooding with 3 injectors and 4 producers. The history matching procedure and models are as described above. In Figure 3-1 we present the "true" pixel-based geological model (top), the "true" DFM (middle), and the history matched DFM (bottom). The well locations are as indicated in Figure 3-1 (top). Figure 3-2 shows the water injection and oil and water production rates on a field basis. The solid black line corresponds to the injection or production rate for the "true" model,

the dashed red line to the initial guess pixel-based model, the dashed blue line to the history matched pixel-based model, and the dashed green line to the history matched DFM (as described above, the history matched DFM is constructed directly from the history matched pixel-based model). It is evident that the match obtained on a field basis is quite satisfactory. Though some amount of error is apparent, a clear improvement relative to the initial guess is achieved. In addition, there is a reasonably close correspondence between the history matched pixel model and the history matched DFM, which suggests that the calibration procedure is acceptable at the field level.

The level of agreement generally degrades when assessed on a well by well basis. In the case of injection wells (Figure 3-3), however, the history matched DFM continues to perform well. Oil and water production rates for each producer are shown in Figure 3-4 and Figure 3-5. These matches are not as good as those observed for field-wide production. In general the oil and water rate results for individual producers show some improvement relative to the initial pixel-based model, although in many cases this improvement is slight. For this example, the procedure appears to have the most difficulty with well by well produced water rates. For two of the production wells, there is significant discrepancy between the history matched pixel model and the history matched DFM, which suggests that some type of recalibration may be useful.

Figure 3-6 shows the behavior of the objective function with iteration. This and subsequent objective functions are computed based on the mismatch between predictions from the current pixel model and the “true” data. We compute the

objective function using the pixel model because we do not construct a DFM until the pixel-based history match is complete. The objective function in Figure 3-6 is seen to decrease by about one order of magnitude, which is consistent with the relatively small improvements in rates observed in the previous figures. For this example the workflow appears to be effective at the field level but only partially effective on a well by well basis.

Example 2

The second case involves waterflooding with 3 injectors and 3 producers. In Figure 3-7 we show the "true" pixel-based geological model with wells (top), the "true" DFM (middle), and the history matched DFM (bottom). The water injection and the oil and water production rates for the field are shown in Figure 3-8. The matches at the field level are seen to be very good. In addition, as was the case in Example 1, the history matched pixel model and the history matched DFM agree closely at the field level.

As seen in the previous example, the match on a well by well basis degrades compared to the field-level match. Figure 3-9 shows the water injection rate for each injector while Figure 3-10 and Figure 3-11 show oil and water production rates for each producer. From Figure 3-10 it is evident that all three injectors show close matches between the "true" data and the matched pixel-based model. However, the rates for the history matched DFM are less accurate for Injectors 1 and 2. The same behavior occurs for oil production rate in all three producers (Figure 3-10). Water production

rates show some error, though the history matched results are much better than the initial guess pixel model, which predicts very little water production. Figure 3-12 displays the decrease in the objective function with iteration. There is slightly more reduction in the objective function in this case than in Example 1.

Example 3

The third case involves waterflooding with 3 injectors and 4 producers. The models and well locations are shown in Figure 3-13. Figure 3-14 shows the water injection and the oil and water production rates on a field basis. For this case the history matched DFM agrees very closely with the "true" data, though it should be noted that the initial guess pixel model provides reasonably accurate results for water injection and oil production rates (but not for water production rate). In addition, there is some discrepancy between the field-wide water production rates for the history matched pixel model and the history matched DFM. Thus the very close agreement between the history matched DFM and the "true" water rate may be somewhat fortuitous.

Individual well injection rates are shown in Figure 3-15. The history matched models (particularly the pixel model) agree closely with the "true" data, though again the initial guess pixel model provides results that are not far from the data. Figure 3-16 shows the oil production rates. The history matching procedure provides little if any improvement for oil production rates (results clearly degrade for one of the wells), though the initial guess pixel model is already fairly accurate. Discrepancies in predictions between the history matched pixel and history matched DFM adversely

affect the level of accuracy of the history matched DFM. Water production rates are shown in Figure 3-17. The history matched DFM shows clear improvement relative to the initial guess pixel model for three of the four production wells. However, the discrepancies between the history matched pixel model and the history matched DFM suggest that this may be partly fortuitous.

The marginal performance observed for this case is reflected in the objective function (Figure 3-18), which decreases by only about a factor of 3. However, the starting point of the objective function for this case is about a factor of 5-10 less than that for the previous two examples. This may suggest that the method in its current form is less effective for improving models that already show relatively little error.

The three examples considered here demonstrate that the overall history matching procedure is reasonably effective in terms of achieving agreement in field-scale quantities, though it is less effective for well by well matches. It is common for history matching procedures to provide better agreement at the field scale than at the well scale. This is because field scale quantities entail averages over the well scale, so there is the possibility for error cancellation. In the next chapter we discuss some aspects of the workflow that should be addressed in future research.

a) true pixel model

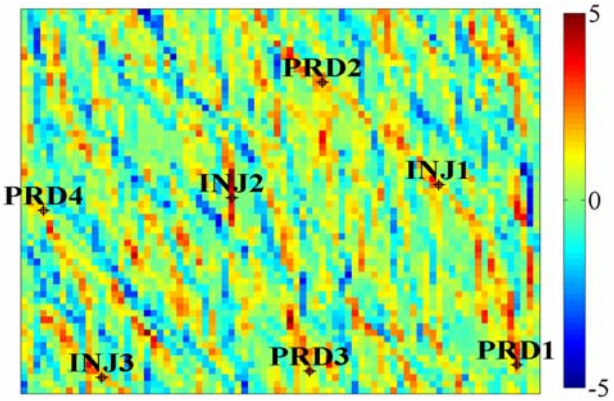

b) true DFM

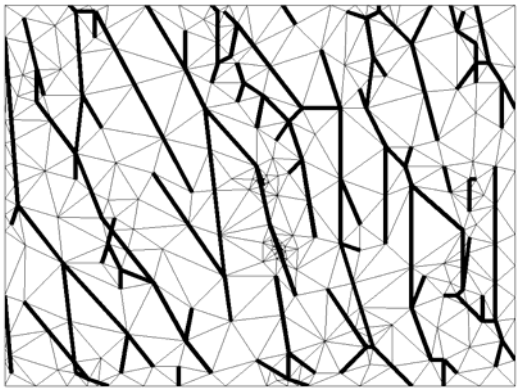

c) matched DFM

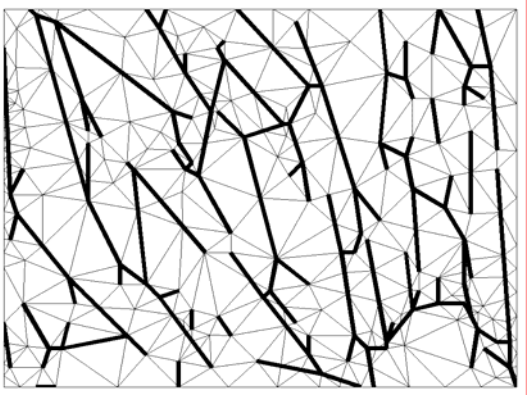

Figure 3-1 Well locations in “true” pixel-based model, and DFMs for “true” and matched models (example 1)

a) field water injection

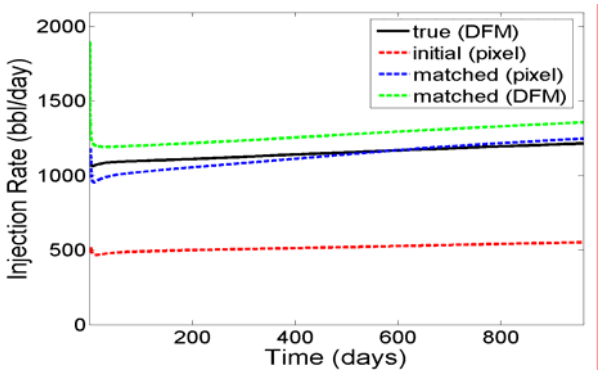

b) field oil production

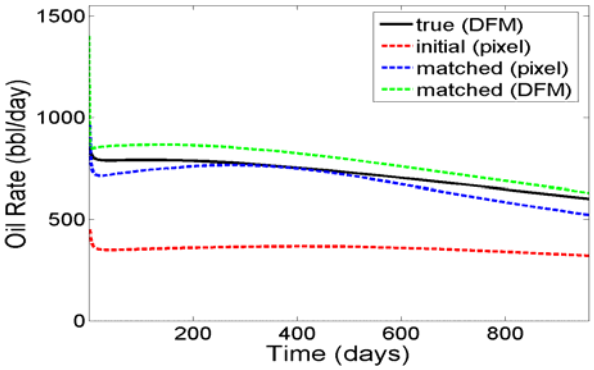

c) field water production

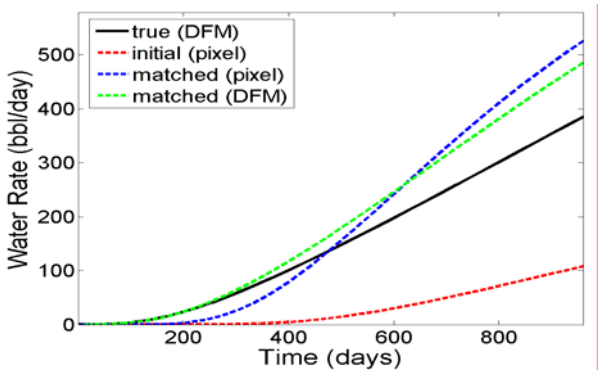

Figure 3-2 Field injecting and producing rates for the true, initial and history matched models (example 1)

a) injector 1

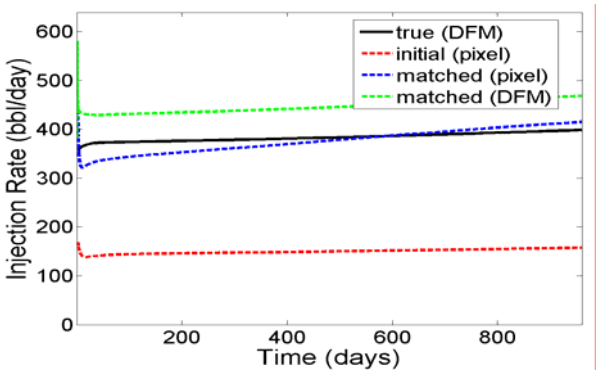

b) injector 2

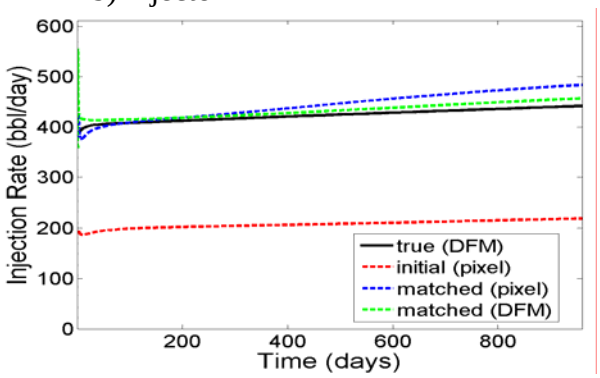

c) injector 3

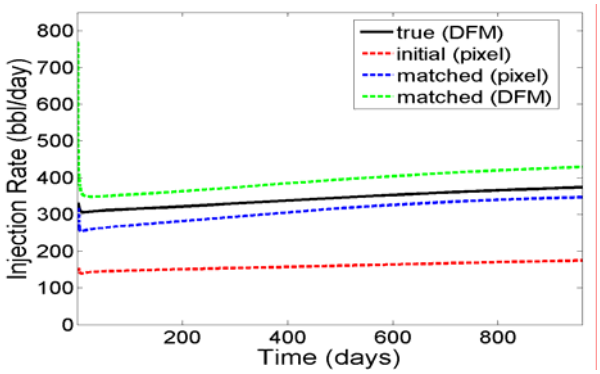

Figure 3-3 Well injection rates for the true, initial and history matched models (example 1)

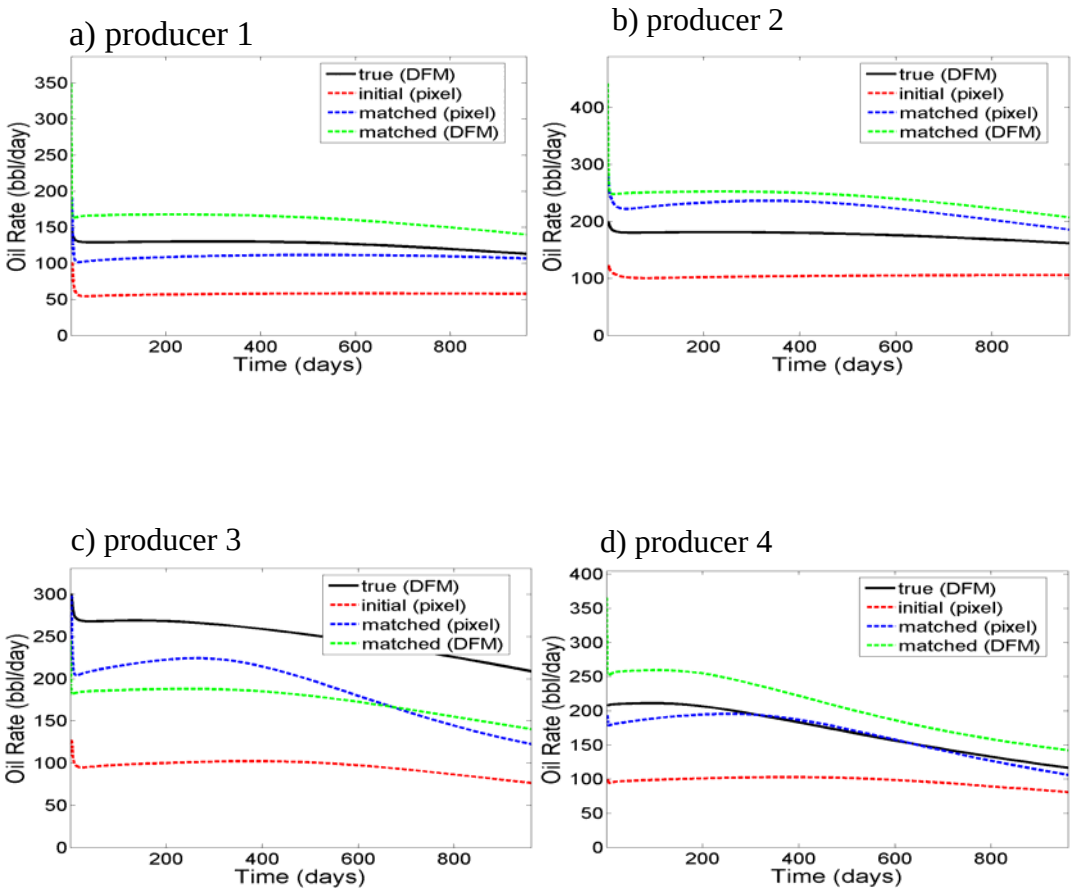

Figure 3-4 Well oil production for the true, initial and history matched models (example 1)

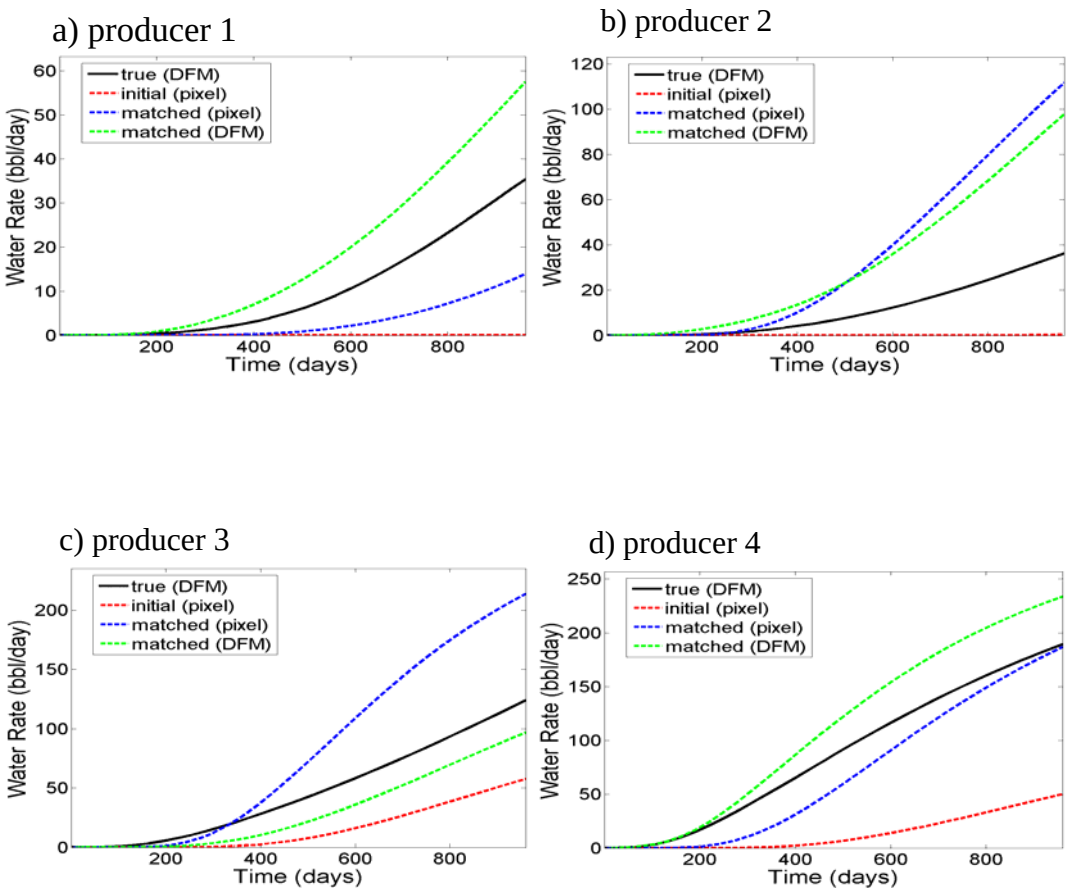

Figure 3-5 Well water production rates for the true, initial and history matched models (example 1)

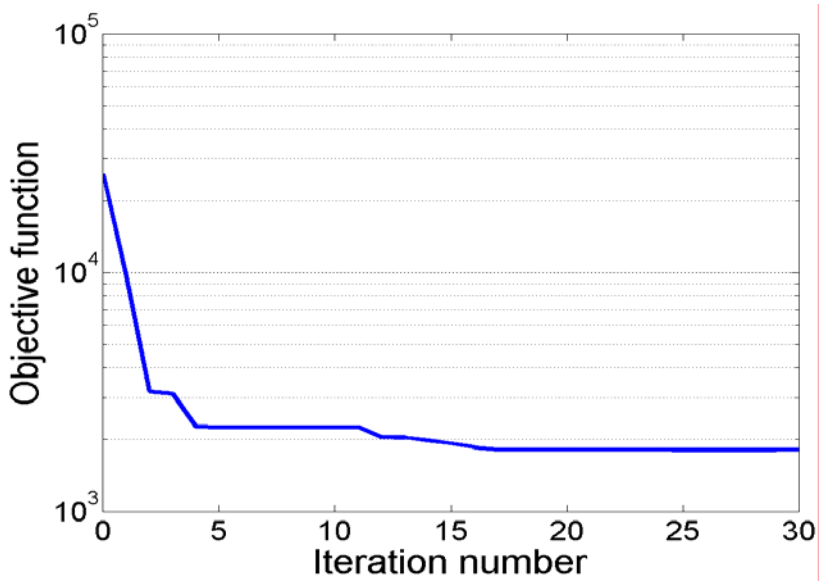

Figure 3-6 Behavior of objective function with iteration number (example 1)

a) true pixel model

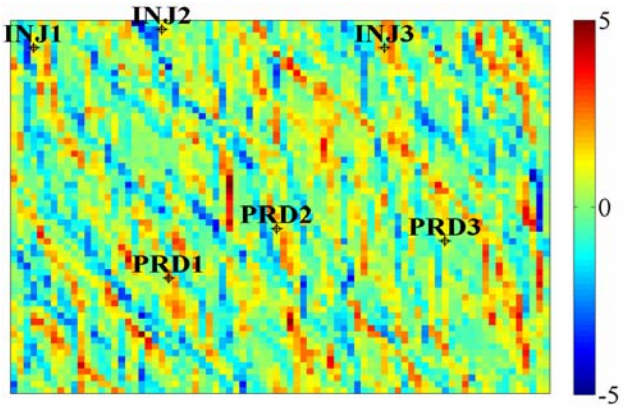

b) true DFM

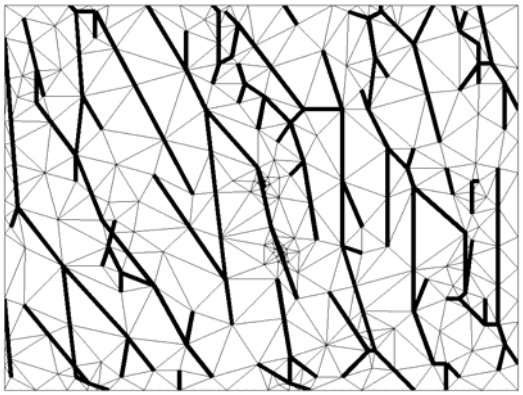

c) matched DFM

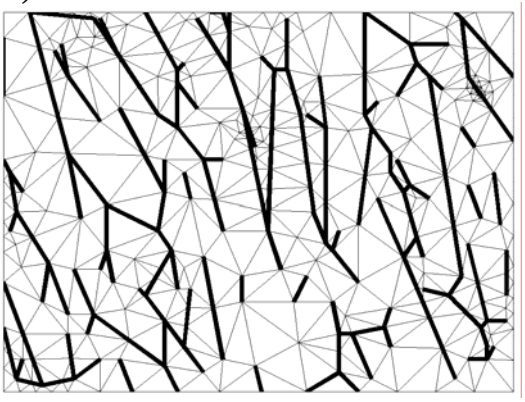

Figure 3-7 Well locations in “true” pixel-based model, and DFMs for “true” and matched models (example 2)

a) field water injection

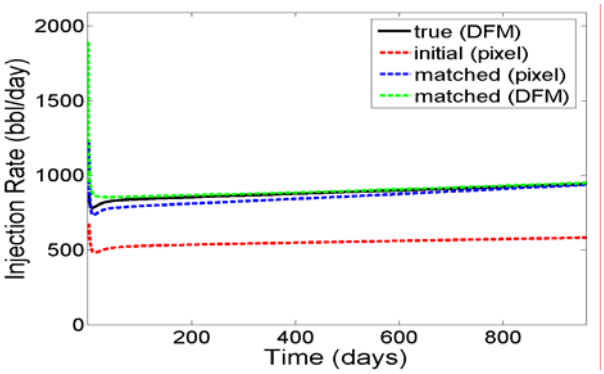

b) field oil production

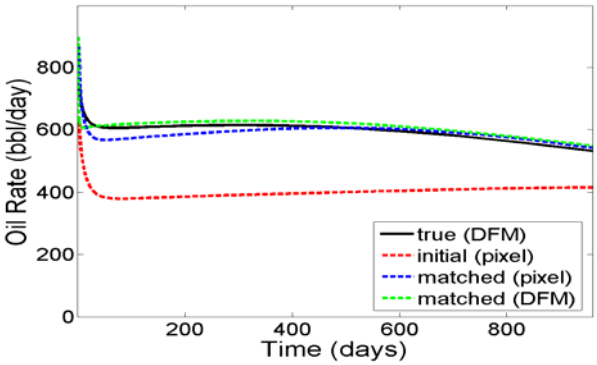

c) field water production

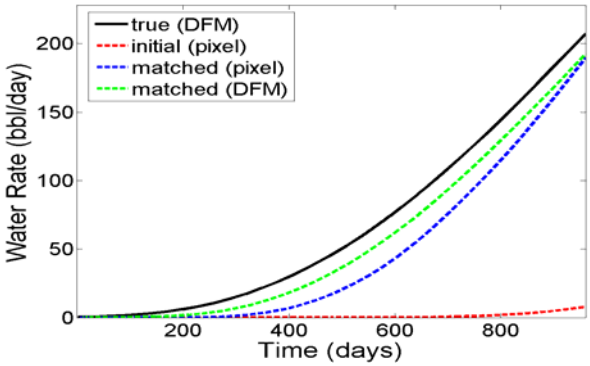

Figure 3-8 Field injecting and producing rates for the true, initial and history matched models (example 2)

a) injector 1

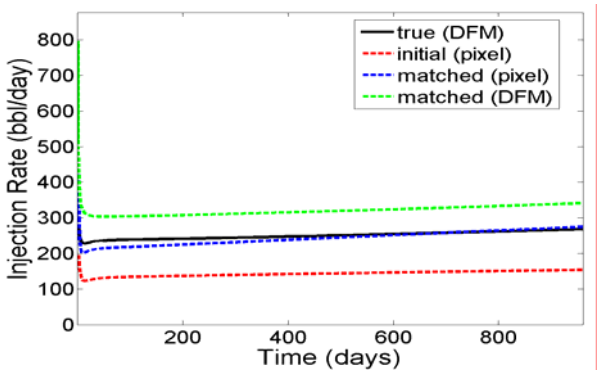

b) injector 2

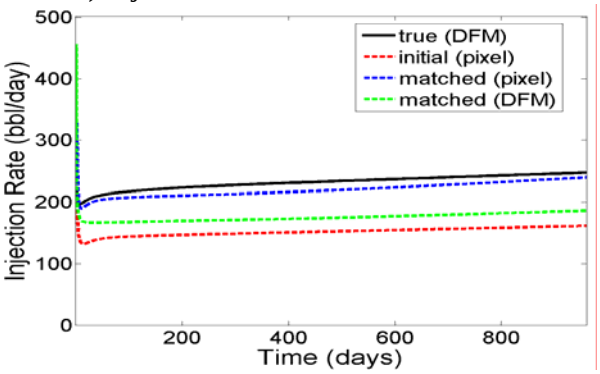

c) injector 3

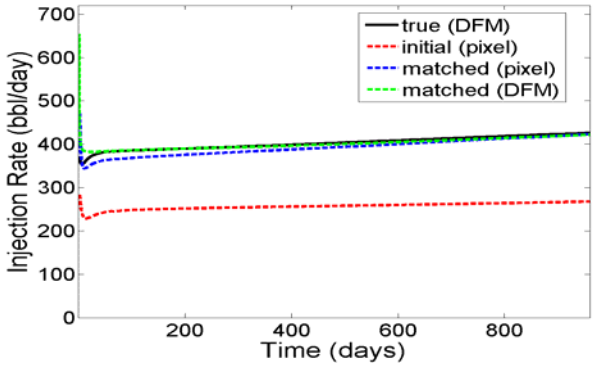

Figure 3-9 Well injection rates for the true, initial and history matched models (example 2)

a) producer 1

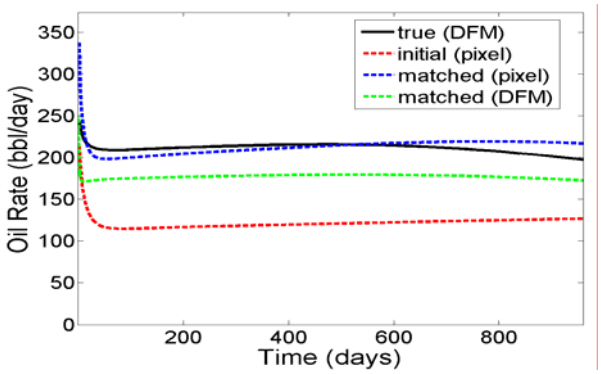

b) producer 2

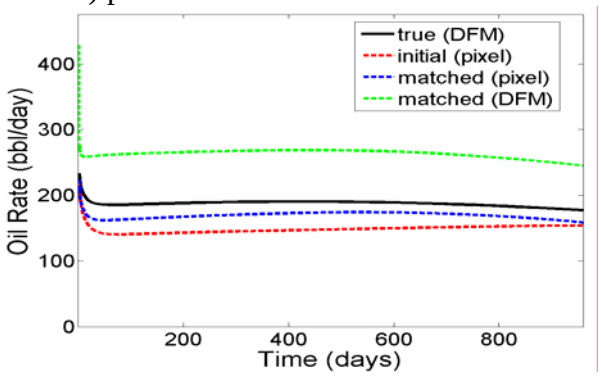

c) producer 3

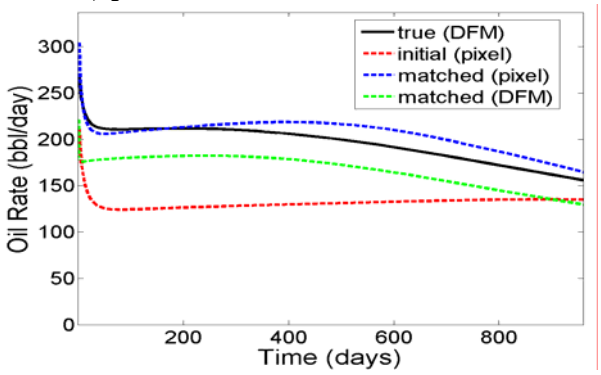

Figure 3-10 Well oil production for the true, initial and history matched models (example 2)

a) producer 1

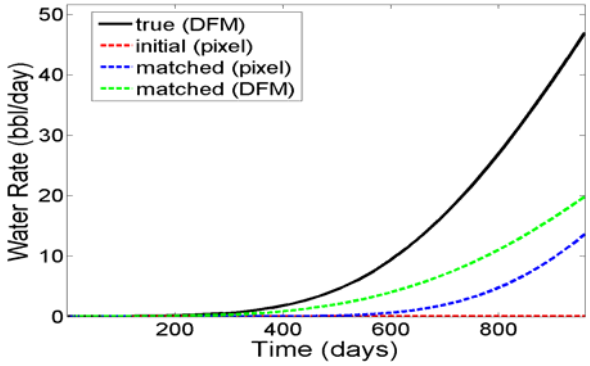

b) producer 2

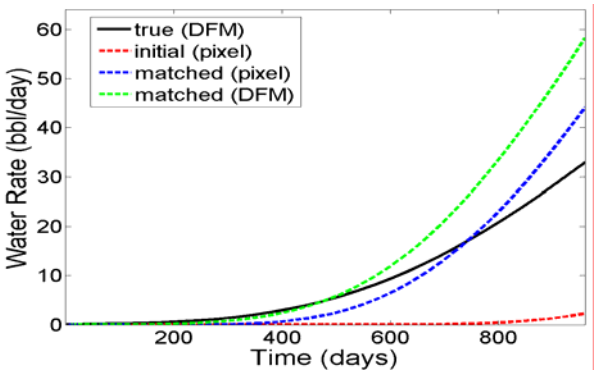

c) producer 3

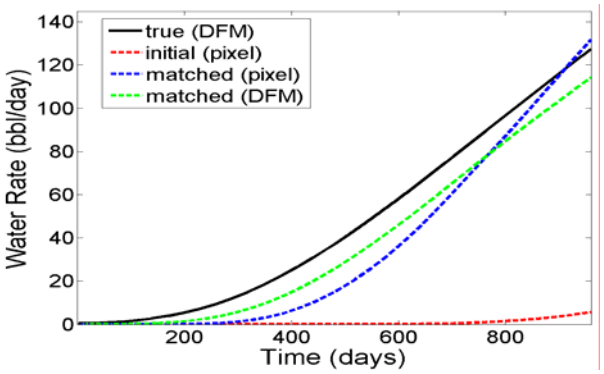

Figure 3-11 Well water production rates for the true, initial and history matched models (example 2)

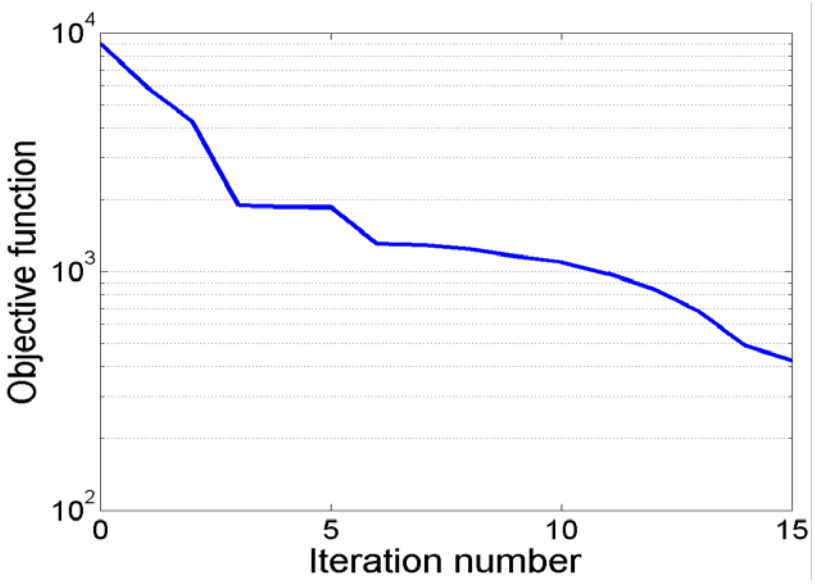

Figure 3-12 Behavior of objective function with iteration number (example 2)

a) true pixel model

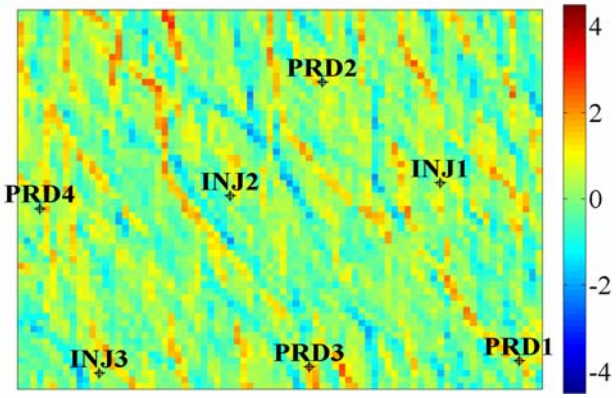

b) true DFM

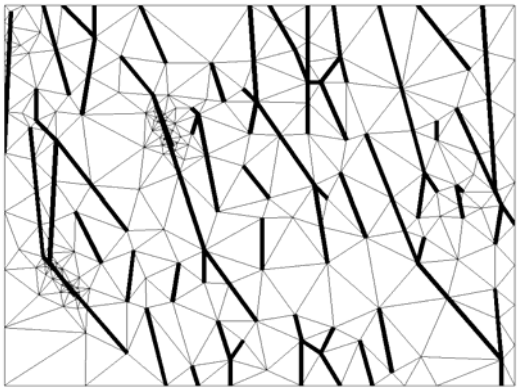

c) matched DFM

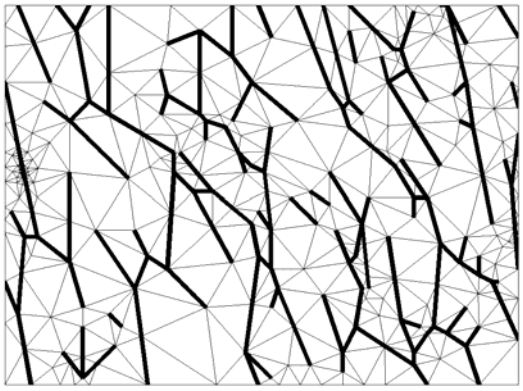

Figure 3-13 Well locations in “true” pixel-based model, and DFMs for “true” and matched models (example 3)

a) field water injection

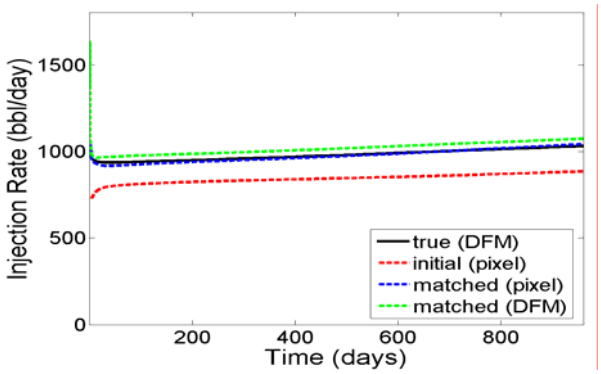

b) field oil production

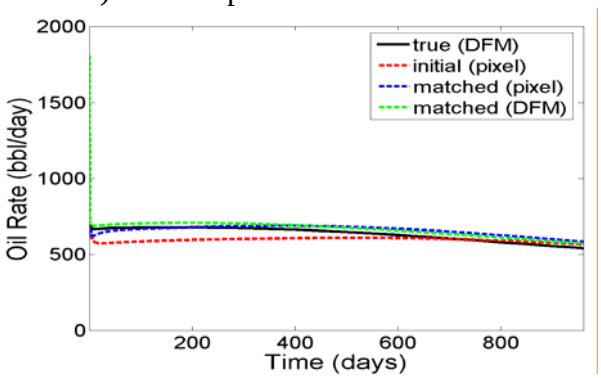

c) field water production

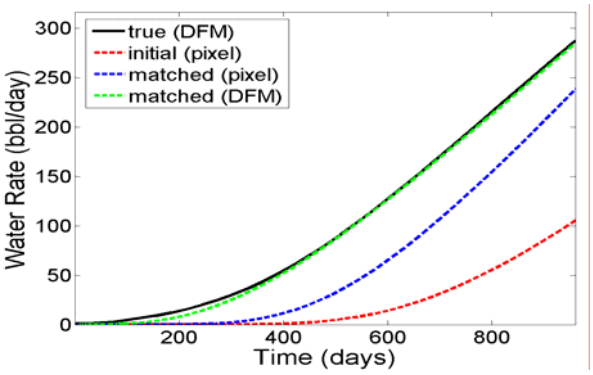

Figure 3-14 Field injecting and producing rates for the true, initial and history matched models (example 3)

a) injector 1

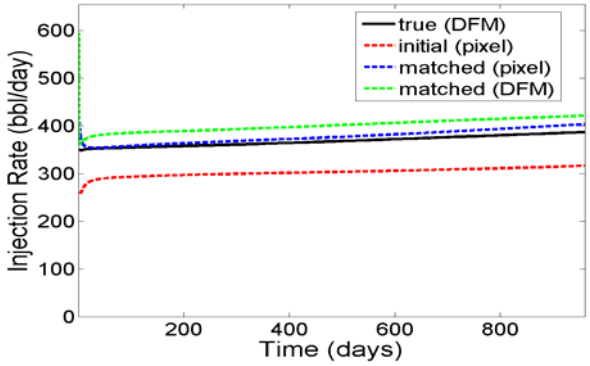

b) injector 2

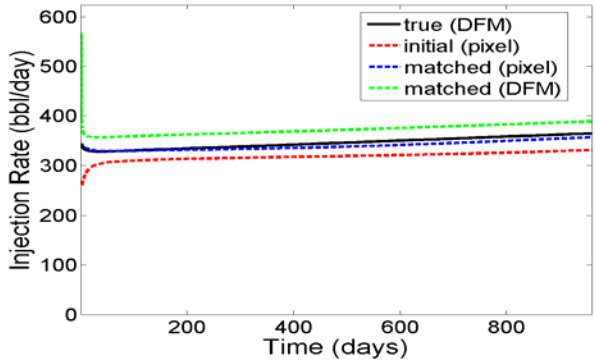

c) injector 3

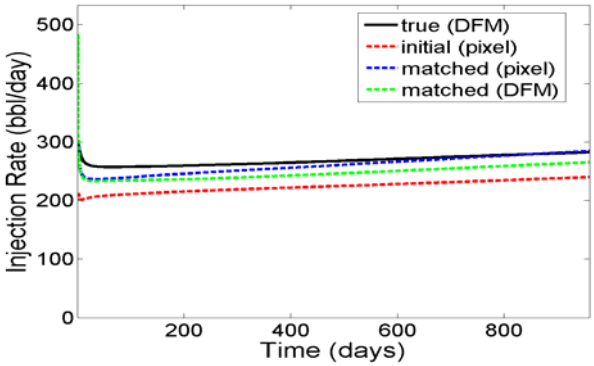

Figure 3-15 Well injection rates for the true, initial and history matched models (example 3)

a) producer 1

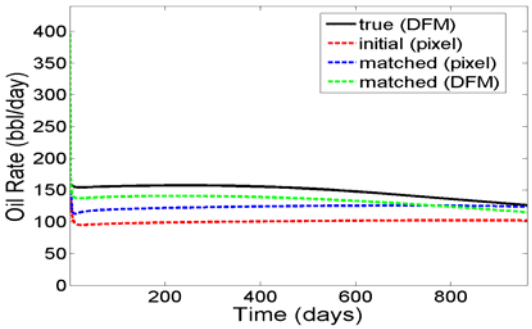

b) producer 2

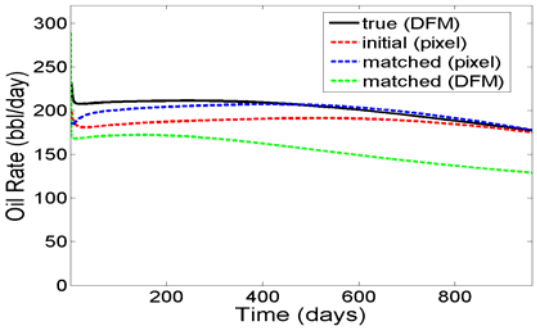

c) producer 3

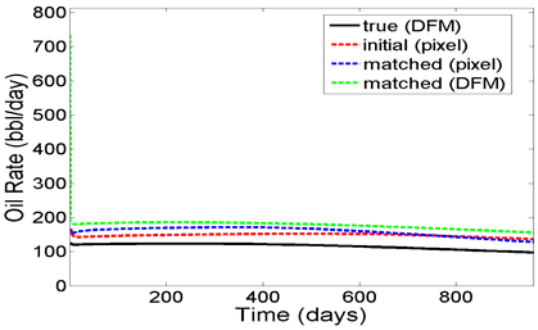

d) producer 4

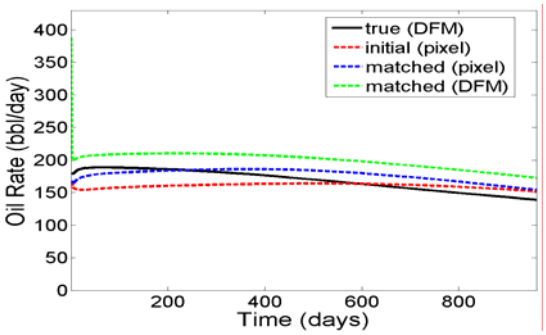

Figure 3-16 Well oil production for the true, initial and history matched models (example 3)

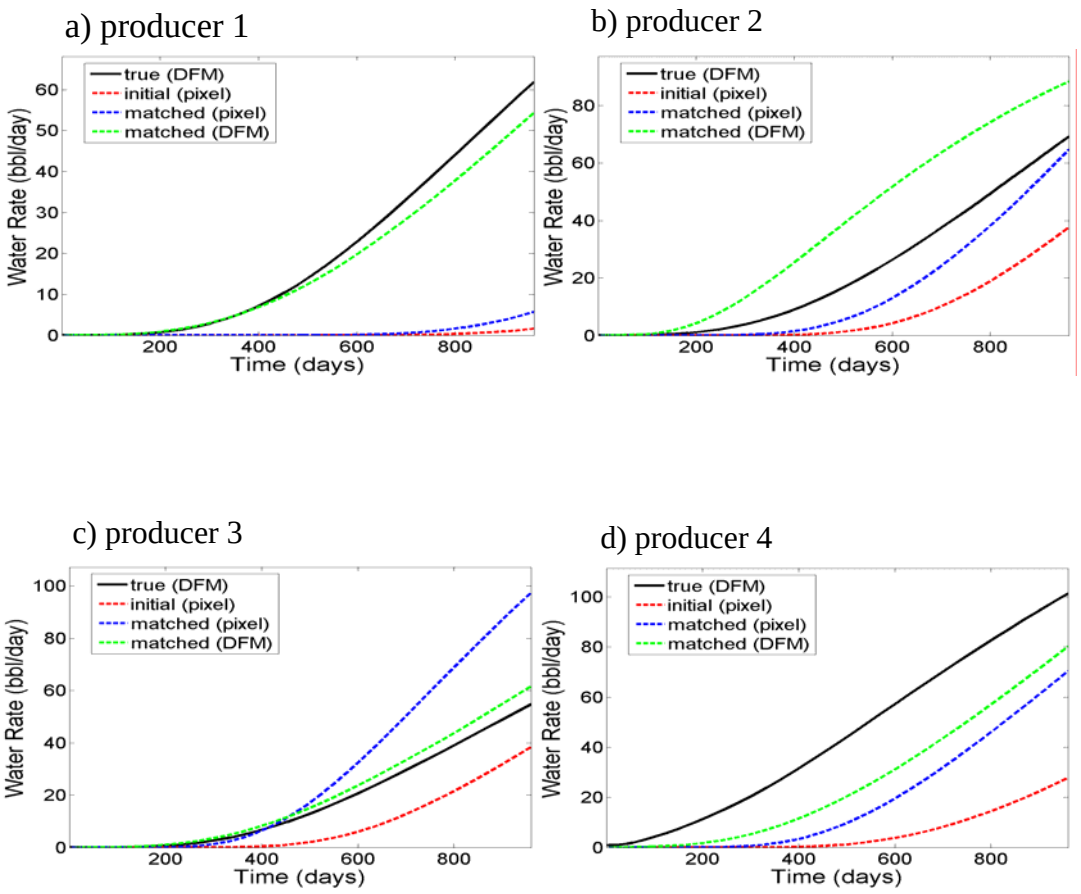

Figure 3-17 Well water production rates for the true, initial and history matched models (example 3)

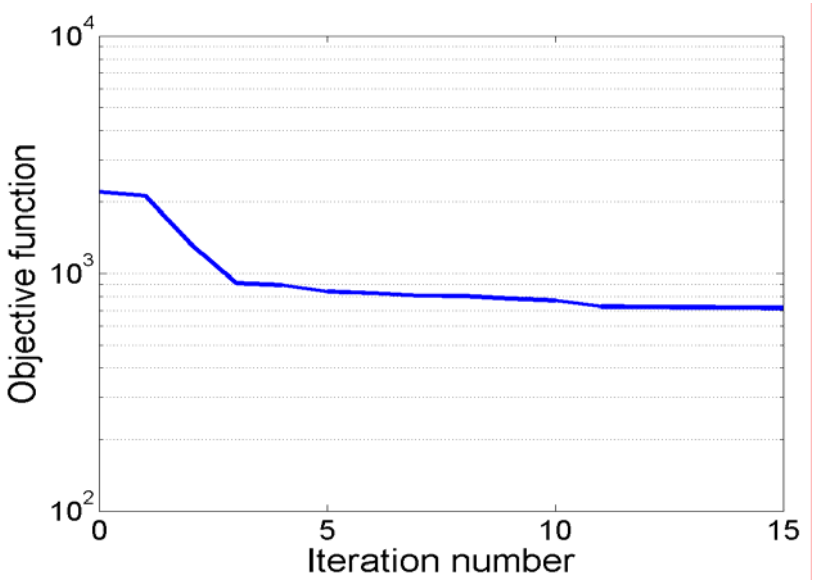

Figure 3-18 Behavior of objective function with iteration number (example 3)

Chapter 4

4. Summary and Future Work

The objective of this work was to develop a prototype workflow for history matching naturally fractured reservoirs. This workflow combines the accuracy of flow modeling using DFMs with the efficiency of KPCA-based history matching. The workflow consists of a two-step approach. The first step entails the calibration of a pixel-based model with its equivalent DFM. The calibration parameters consist of a set of coefficients used to determine the grid block permeabilities and porosities for pixel-based models. The second step exploits the efficiency of the gradient-based KPCA history matching by direct application of this method to pixel-based models, where grid block permeabilities and porosities are assigned to each block using the calibration established in the first step.

The methods were applied as stand-alone procedures for test cases on two-dimensional reservoir models. Waterflooding involving several wells was considered. Both the KPCA history matching and the calibration techniques were shown to provide reasonable results, particularly at the field level. The overall history matching workflow was then tested. The method was observed to be reasonably effective in

achieving field-level agreement in total injection rate and oil and water production rates. The level of agreement degraded, however, in some cases considerably, for the well by well results. The overall method is, we believe, quite promising, though several aspects require additional investigation. These include the following:

- A key aspect of the overall workflow is the correspondence in flow results between a pixel-based model and its equivalent DFM. The calibration procedure aims to establish this correspondence. As explained in Chapter 3, in the examples presented here we established this correspondence using the "true" DFM and the "true" pixel model. In real applications the true model is not known, so an alternative approach is required. Such an approach, which might include calibration over multiple models generated randomly or some amount of recalibration during the history match, should be developed and evaluated.

- The calibration accuracy is also affected by the image processing technique used to obtain a DFM from a pixel model. The current method detects only the ends and intersections of the fractures and represents the fractures with straight segments. This limits our ability to represent fractures with complex geometries. Improved procedures for extracting the DFM from continuous pixel images should be investigated.

- In the DFM, different relative permeability curves are used for the matrix and the fractures. The relative permeability curves used for the pixel-based model

during the calibration step are specified to be the matrix relative permeabilities. It may be better to incorporate additional calibration parameters that would allow for the use of optimized “effective” relative permeabilities for the pixel-based model rather than prescribe these to be the matrix relative permeabilities.

- The calibration procedure (which might include parameters defining “effective” relative permeabilities) may be useful for other aspects of fracture modeling, such as for the optimization of well settings in NFRs. In this sense a calibrated coarse-scale pixel model could be used as a surrogate or proxy model for the full DFM. The robustness and accuracy of the calibration for changing well rates, different well locations, etc. should be assessed and enhanced as necessary.

- In KPCA, models in physical space are obtained from feature space representations by solving a pre-image problem, as described in Sarma et al. (2008). There are some issues associated with this pre-image problem that require further investigation. For example, the pre-image with polynomial kernels is in general nonunique, and this can impact the model generation and history matching procedures. This is less of a problem with the second-order polynomial kernels applied here, though it may be a significant concern if we apply third or higher order polynomials. Higher order kernels may be useful as they are able to provide more distinct fracture-like features in the pixel models. Therefore issues surrounding the use of higher order kernels should be

investigated. We also encountered some problems in controlling the degree of variability in the pre-images. This may also require further study.

- The examples considered here were all two-dimensional models. More realistic three-dimensional cases should also be tested.

We expect that, once the issues highlighted above are successfully addressed, our technique could become a viable procedure for history matching naturally fractured reservoirs.

Nomenclature

c	Calibration parameters
$\mathbf{c}$	Vector of calibration parameters
$\mathbf{C}$	Covariance matrix
d	Maximum order of polynomial kernel
erf	Error function
F	Higher order space or feature space
g	Flow simulation equations
k	Kernel function
k_x	Permeability in x-direction
k_y	Permeability in y-direction
$\mathbf{K}$	Kernel matrix
l	Number of basis functions
$\mathbf{m}$	Parameters of reservoir model
$\overline{\mathbf{m}}$	Average of the random field
$\tilde{\mathbf{m}}$	Model in high order space
N	Number of time steps
N_C	Number of grid blocks in simulation model
N_R	Number of realizations
O	Objective function for calibration
P_{DFM}	Production from DFM
P_{obs}	Actual observed data
P_{pixel}	Production from pixel-based model
P_{sim}	Simulated production
R^{N_C}	Original space of realization
S	Objective function for history matching

$\mathbf{v}$	Eigenvector of covariance matrix
$\mathbf{x}$	Dynamic states

Greek

ε	Perturbation used for numerical derivatives
ϕ	Porosity
$\mathbf{\Phi}$	Basis function
$\tilde{\mathbf{\Phi}}$	Basis function in feature space
φ	Pre-image values after transformation with error function
λ	Eigenvalue
ξ	Independent random variables for K-L expansion
$\boldsymbol{\xi}$	Vector of random variables for K-L expansion
ψ	Pre-image values

Subscripts

0	Initial condition
DFM	Discrete fracture model
i	Summation index, element index, vector component index
ij	Matrix element
j	Summation index, vector component index
k	Vector component index
n	Summation index
obs	Observed value
pixel	Pixel-based model
sim	Simulated value

Superscripts

0	Time step zero
n	Time step, order of polynomial kernel

T	Transpose of matrix or vector

Abbreviations

BHP	Well bottom hole pressure
DFM	Discrete fracture model
EnKF	Ensemble Kalman filter
GPRS	General purpose research simulator
K-L	Karhunen-Loeve
KPCA	Kernel principal component analysis
MSR	Multiple subregion
NFR	Naturally fractured reservoir
PCA	Principal Component Analysis
SPSA	Simultaneous perturbation stochastic approximation
SQP	Sequential quadratic programming
SVD	Singular value decomposition

References

Agarwal, B. and Blunt, M.J. 2003. Streamline-Based Method with Full-Physics Forward Simulation for History-Matching Performance Data of a North Sea Field. *SPEJ* **8** (2): 171-180. SPE-84952-PA.

Anterion, F., Eymard, R., and Karcher, B. 1989. Use of Parameter Gradients for Reservoir History Matching. Paper SPE 18433 presented at the Reservoir Simulation Symposium, Houston, Texas, 6-8 February.

Baca, R.G., Arnett, R.C., and Langford, D.W. 1984. Modelling Fluid Flow in Fractured-Porous Rock Masses by Finite-Element Techniques. *International Journal of Numerical Methods Fluids* **4** (4): 337-348.

Bissell, R. 1994a. Calculating Optimal Parameters for History Matching. *Proc.*, 4th European Conference on the Mathematics of Oil Recovery, Roros, Norway.

Bissell, R.C., Sharma, Y., and Killough, J.E. 1994b. History Matching Using the Method of Gradients: Two Case Studies. Paper SPE 28590 presented at the Annual Technical Conference and Exhibition, New Orleans, Louisiana, 25-28 September.

Bissell, R.C., Dubrule, O., Lamy, P., Swaby, P., and Lepine, O. 1997. Combining Geostatistical Modelling With Gradient Information for History Matching: The Pilot Point Method. Paper SPE 38730 presented at the Annual Technical Conference and Exhibition, San Antonio, Texas, 5-8 October.

Cacas, M.C., Daniel, J.M., and Letouzey, J. 2001. Nested Geological Modeling of Naturally Fractured Reservoirs. *Petroleum Geoscience* **7** (Supplement): 43-52.

Caers, J. 2003a. Efficient Gradual Deformation Using a Streamline-based Proxy Method. *Journal of Petroleum Science and Engineering* **39** (1-2): 57-83.

Caers, J. 2003b. History Matching Under Training Image-based Geological Model Constraints. *SPEJ* **8** (3): 218-226. SPE-74716-PA.

Cao, H. 2002. Development of Techniques for General Purpose Simulators. PhD dissertation, Stanford University, Stanford, California.

Carter, R.D., Kemp, L.F., Pierce, A.C., and Williams, D.L. 1974. Performance Matching With Constraints. *SPEJ* **14** (2): 187-196. SPE-4260-PA.

Chavent, G.M., Dupuy, M., and Lemonnier, P. 1975. History Matching by Use of Optimal Control Theory. *SPEJ* **15** (1): 74-86. SPE-4627-PA.

Chen, W.H., Gavalas, G.R., Seinfeld, J.H., and Wasserman, M.L. 1974. A New Algorithm for Automatic History Matching. *SPEJ* **14** (6): 593-608. SPE-4545-PA.

Cheng, H., Wen, X.H., Milliken, W.J., and Datta-Gupta, A. 2004. Field Experiences with Assisted and Automatic History Matching Using Streamline Models. Paper SPE 89857 presented at the Annual Technical Conference and Exhibition, Houston, Texas, 26-29 September.

Cui, H. and Kelkar, M. 2005. Automatic History Matching of Naturally Fractured Reservoirs and a Case Study. Paper SPE 94037 presented at the Western Regional Meeting, Irvine, California, 30 March-1 April.

Dong, Y., Gu, Y., and Oliver, D.S. 2006. Sequential Assimilation of 4D Seismic Data for Reservoir Description Using the Ensemble Kalman Filter. *Journal of Petroleum Science and Engineering* **53** (1-2): 83-99.

Flodin, E.A. and Aydin, A. 2004. Evolution of a Strike-Slip Fault Network, Valley of Fire State Park, Southern Nevada. *Geological Society of America Bulletin* **116** (1): 42-59.

Gang, T. and Kelkar, M. 2006. Efficient History Matching in Naturally Fractured Reservoirs. Paper SPE 99578 presented at the Symposium on Improved Oil Recovery, Tulsa, Oklahoma, 22-26 April.

Gao, G., Zafari, M., and Reynolds, A.C. 2005. Quantifying Uncertainty for the PUNQ-S3 Problem in a Bayesian Setting with RMI and EnKF. Paper SPE 93324 presented at the Reservoir Simulation Symposium, Houston, Texas, 31 January-2 February.

Gao, G., Li, G., and Reynolds, A.C. 2007. A Stochastic Optimization Algorithm for Automatic History Matching. *SPEJ* **12** (2): 196-208. SPE-90065-PA.

Gavalas, G.R., Shah, P.C., and Seinfeld, J.H. 1976. Reservoir History Matching by Bayesian Estimation. *SPEJ* **16** (6): 337-350. SPE-5740-PA.

Gilman, J.R. and Kazemi, H. 1983. Improvements in Simulation of Naturally Fractured Reservoirs. *SPEJ* **23** (4): 695-707. SPE-10511-PA.

Gong, B., Karimi-Fard, M., and Durlofsky, L.J. 2006. An Upscaling Procedure for Constructing Generalized Dual-Porosity/Dual Permeability Model from Discrete Fracture Characterizations. Paper SPE 102491 presented at the Annual Technical Conference and Exhibition, San Antonio, Texas, 24-27 October.

Granet, S., Fabrie, P., Lemonnier, P., and Quintard, M. 2001. A Two-phase Flow Simulation of a Fractured Reservoir Using a New Fissure Element Method. *Journal of Petroleum Science and Engineering* **32** (1): 35-52.

Haralick, R.M. and Shapiro, L.G. ed. 1992. *Computer and Robot Vision, Volume I*. Reading, Massachusetts: Addison-Wesley Publishing Company.

He, N., Reynolds, A.C., and Oliver, D.S. 1997. Three-Dimensional Description from Multiwell Pressure Data and Prior Information. *SPEJ* **2** (3): 312-327. SPE-36509-PA.

Hu, L.Y., Blanc, G., and Noetinger, B. 2001. Gradual Deformation and Iterative Calibration of Sequential Stochastic Simulations. *Mathematical Geology* **33** (4): 475-489.

Hu, L.Y. and Jenni, S. 2005. History Matching of Object-Based Stochastic Reservoir Models. *SPEJ* **10** (3): 312-323. SPE-81503-PA.

Jacquard, P. 1965. Permeability Distribution from Field Pressure Data. *SPEJ* **5** (4): 281-294. SPE-1307-PA.

Jahns, H.O. 1966. A Rapid Method for Obtaining a Two Dimensional Description from Well Response Data. *SPEJ* **6** (4): 315-327. SPE-1473-PA.

Jenni, S., Hu, L.Y., Basquet, R., Marsily, G., and Bourbiaux, B. 2004. History Matching of Stochastic Models of Field-Scale Fractures: Methodology and Case Study. Paper SPE 90020 presented at the Annual Technical Conference and Exhibition, Houston, Texas, 26-29 September.

Juanes, R., Samper, J., and Molinero, J. 2002. A General and Efficient Formulation of Fractures and Boundary Conditions in the Finite Element Method. *International Journal of Numerical Methods Engineering* **54** (12): 1751-1774.

Karimi-Fard, M. and Firoozabadi, A. 2001. Numerical Simulation of Water Injection in 2D Fractured Media Using Discrete-Fracture Model. Paper SPE 71615

presented at the Annual Technical Conference and Exhibition, New Orleans, Louisiana, 30 September-3 October.

Karimi-Fard, M., Durlofsky, L.J., and Aziz, K. 2004. An Efficient Discrete Fracture Model Applicable for General-Purpose Reservoir Simulators. *SPEJ* **9** (2): 227-236. SPE-88812-PA.

Karimi-Fard, M., Gong, B., and Durlofsky, L.J. 2006. Generation of Coarse-Scale Continuum Flow Models from Detailed Fracture Characterizations. *Water Resources Research* **42** (10): W10423.

Kazemi, H., Merrill, L.S., Porterfield, K.L., and Zeman, P.R. 1976. Numerical Simulation of Water-Oil Flow in Naturally Fractured Reservoirs. *SPEJ* **16** (6): 317-326. SPE-5719-PA.

Kim, J.G. and Deo, M.D. 2000. Finite Element, Discrete-fracture Model for Multiphase Flow in Porous Media. *AIChEJ* **46** (6) 1120-1130.

Kleppe, J. and Morse, R.A. 1974. Oil Production from Fractured Reservoirs by Water Displacement. Paper SPE 5084 presented at the Annual Meeting, Houston, Texas, 6-9 October.

Landa, J.L., Kamal, M.M., Jenkins, C.D., and Horne, R.N. 1996. Reservoir Characterization Constrained to Well Test Data: A Field Example. Paper SPE 36511 presented at the Annual Technical Conference and Exhibition, Denver, Colorado, 6-9 October.

Laubach, S.E. 1991. Fracture Patterns in Low Permeability Sandstone Gas Reservoir Rocks in the Rocky Mountain Region. Paper SPE 21853 presented at the Low Permeability Reservoir Symposium, Denver, Colorado, 15-17 April.

Lee, T.Y. and Seinfeld, J.H. 1987. Estimation of Two-Phase Petroleum Reservoir Properties by Regularization. *Journal of Computational Physics* **69** (2): 397-419.

Le Gallo, Y. and Le Ravalec-Dupin, M. 2000. History Matching Geostatistical Reservoir Models with Gradual Deformation Method. Paper SPE 62922 presented at the Annual Technical Conference and Exhibition, Dallas, Texas, 1-4 October.

Li, R., Reynolds, A.C., and Oliver, D.S. 2001. History Matching of Three-Phase Flow Production Data. Paper SPE 66351 presented at the Reservoir Simulation Symposium, Houston, Texas, 11-14 February.

Lindquist, W.B., Lee, S.M., Coker, D.A., Jones, K.W., and Spanne, P. 1996. Medial Axis Analysis of Void Structure in Three-Dimensional Tomographic Images of Porous Media. *Journal of Geophysical Research* **101** (B4): 8297-8310.

Liu, N. and Oliver, D.S. 2004. Automatic History Matching of Geologic Facies. *SPEJ* **9** (4): 429-436. SPE-84594-PA.

Liu, N. and Oliver, D.S. 2005. Critical Evaluation of the Ensemble Kalman Filter on History Matching of Geologic Facies. Paper SPE 92867 presented at the Reservoir Simulation Symposium, Houston, Texas, 31 January-2 February.

Mathworks. 2006. *Optimization Toolbox: For Use with Matlab*. Natick, Massachusetts: The Mathworks Inc.

Matthäi, S.K., Mezentsev, A., and Belayneh, M. 2007. Finite Element-Node-Centered Finite-Volume Two-Phase-Flow Experiments with Fractured Rock Represented by Unstructured Hybrid-Element Meshes. *SPEREE* **10** (6): 740-756. SPE-93341-PA.

Oliver, D.S. 1996. Multiple Realizations of the Permeability Field from Well Test Data. *SPEJ* **1** (2): 145-154. SPE-27970-PA.

Pollard, D. and Segall, P. 1987. Theoretical Displacements and Stress Near Fractures in Rock, With Applications of Faults, Joints, Veins, Dikes, and Solution Surfaces. In *Fracture Mechanics of Rock*, ed. B. Atkinson, 227-350. London, England: Academic Press.

Pratt, W.K. ed. 2007. *Digital Image Processing*. Hoboken, New Jersey: John Wiley & Sons, Inc.

Rangel-German, E.R. 1999. Experimental and Theoretical Investigation of Multiphase Flow in Fractured Porous Media. MS thesis, Stanford University, Stanford, California.

Reynolds, A.C., He, N., Chu, L., and Oliver, D.S. 1996. Reparameterization Techniques for Generating Reservoir Descriptions Conditioned to Variograms and Well-Test Pressure Data. *SPEJ* **1** (4): 413-426. SPE-30588-PA.

Roggero, F. and Hu, L.Y. 1998. Gradual Deformation of Continuous Geostatistical Models for History Matching. Paper SPE 49004 presented at the Annual Technical Conference and Exhibition, New Orleans, Louisiana, 27-30 September.

Sahni, I. and Horne, R.N. 2006. Stochastic History Matching and Data Integration for Complex Reservoirs Using a Wavelet-Based Algorithm. Paper SPE 103107 presented at the Annual Technical Conference and Exhibition, San Antonio, Texas, 24-27 September.

Sarma, P., Durlofsky, L.J., Aziz, K., and Chen, W.H. 2006. Efficient Real-Time Reservoir Management Using Adjoint-Based Optimal Control and Model Updating. *Computational Geoscience* **10** (1): 3-36.

Sarma, P., Durlofsky, L.J., Aziz, K., and Chen, W.H. 2007. A New Approach to Automatic History Matching Using Kernel PCA. Paper SPE 106176 presented at the Reservoir Simulation Symposium, Houston, Texas, 26-28 February.

Sarma, P., Durlofsky, L.J., and Aziz, K. 2008. Kernel Principal Component Analysis for an Efficient, Differentiable Parameterization of Multiple Point Geostatistics. *Mathematical Geosciences* **40** (1): 3-32.

Schölkopf, B. and Smola, A.J. 2002. *Learning with Kernels*. Cambridge: MIT Press.

Shewchuk, J.R. 1996. Triangle: Engineering a 2D Quality Mesh Generator and Delaunay Triangulator. In *Applied Computational Geometry: Towards Geometric Engineering*, ed. M.C. Lin and D. Manocha, Vol. 1148, 203-222. Berlin: Springer-Verlag.

Smith, R.A.W. and Tan, T.B. 1993. Reservoir Characterization of a Fractured Reservoir Using Automatic History Matching. Paper SPE 25251 presented at the Reservoir Simulation Symposium, New Orleans, Louisiana, 28 February-3 March.

Strebelle, S.B. and Journel, A.G. 2001. Reservoir Modeling Using Multiple-Point Statistics. Paper SPE 71324 presented at the Annual Technical Conference and Exhibition, New Orleans, Louisiana, 30 September-3 October.

Suzuki, S. 2004. History Matching of Naturally Fractured Reservoir Using Elastic Stress Simulation, FracPerm Model and the Probability Perturbation Method. Summer Report, Stanford University, Stanford, California.

Tang, Y.N., Chen, Y.M., Chen, W.H., and Wasserman, M.L. 1989. Generalized Pulse-Spectrum Technique for 2D and 2-Phase History Matching. *Applied Numerical Mathematics* **5** (6): 529-539.

Vasco, D.W., Yoon, S., and Datta-Gupta, A. 1998. Integrating Dynamic Data into High-resolution Reservoir Models using Streamline-Based Analytical Sensitivity Coefficients. Paper SPE 49002 presented at the Annual Technical Conference and Exhibition, New Orleans, Louisiana, 27-30 September.

Vitel, S. 2007. Méthodes de Discrétisation et de Changement d'échelle pour les Réservoirs Fracturés 3D. PhD dissertation, Nancy Université, Institut National Polytechnique de Lorraine, France.

Wang, Y. and Kovscek, A.R. 2000. Streamline Approach for History Matching Production Data. *SPEJ* **5** (4): 353-362. SPE-58350-PA.

Warren, J.E. and Root, P.J. 1963. The Behavior of Naturally Fractured Reservoirs. *SPEJ* **3** (3): 245-255. SPE-426-PA.

Wasserman, M.L., Emanuel, A.S., and Seinfeld, J.H. 1975. Practical Applications of Optimal-Control Theory to History-Matching Multiphase Simulator Models. *SPEJ* **15** (4): 347-355. SPE-5020-PA.

Watson, A.T., Seinfeld, J.H., Gavalas, G.R., and Woo, P.T. 1980. History Matching in Two-Phase Petroleum Reservoirs. *SPEJ* **20** (6): 521-532. SPE-8250-PA.

Wen, X.H., Deutsch, C.V., and Cullick, A.S. 1998. Integrating Pressure and Fractional Flow Data in Reservoir Modeling with Fast Streamline-Based Inverse Method. Paper SPE 48971 presented at the Annual Technical Conference and Exhibition, New Orleans, Louisiana, 27-30 September.

Wen, X.H. and Chen, W.H. 2007. Some Practical Issues on Real-Time Reservoir Model Updating Using Ensemble Kalman Filter. *SPEJ* **12** (2): 156-166. SPE-111571-PA.

Wu, Z., Reynolds, A.C., and Oliver, D.S. 1999. Conditioning Geostatistical Models to Two-Phase Production Data. *SPEJ* **4** (2): 142-155. SPE-56855-PA.

Wu, Z. 2001. A Newton-Raphson Iterative Scheme for Integrating Multiphase Production Data into Reservoir Models. *SPEJ* **6** (3): 343-351. SPE-74143-PA.

Wu, Z. and Datta-Gupta, A. 2002. Rapid History Matching Using a Generalized Travel Time Inversion Method. *SPEJ* **7** (2): 113-122. SPE-78359-PA.

Yadav, S., Srinivasan, S., Bryant, S.L., and Barrera, A. 2005. History Matching Using Probabilistic Approach in a Distributed Computing Environment. Paper SPE 93399 presented at the Reservoir Simulation Symposium, Houston, Texas, 31 January-2 February.

Yang, P.H. and Watson, A.T. 1988. Automatic History Matching with Variable-Metric Methods. *SPERE* **3** (3): 995-1001. SPE-16977-PA.

Zhang, F. and Reynolds, A.C. 2002. Optimization Algorithms for Automatic History Matching of Production Data. *Proc.*, 8th European Conference on the Mathematics of Oil Recovery, Freiberg, Germany.

Zhang, T., Bombarde, S., Strebelle, S., and Oatney, E. 2006. 3D Porosity Modeling of a Carbonate Reservoir Using Continuous Multiple-Point Statistics Simulation. *SPEJ* **11** (3): 375-379. SPE-96308-PA.